

# Fluid phase behavior of nitrogen + acetone and oxygen + acetone by molecular simulation, experiment and the Peng-Robinson equation of state

Thorsten Windmann<sup>1</sup>, Matthias Linnemann<sup>1</sup>, Jadran Vrabec<sup>\*1</sup>

<sup>1</sup> Lehrstuhl für Thermodynamik und Energietechnik, Universität Paderborn, Warburger Straße  
100, 33098 Paderborn, Germany

## Abstract

Vapor-liquid equilibria (VLE) of the binary mixtures nitrogen + acetone and oxygen + acetone are studied by molecular simulation and experiment. A force field model for pure acetone ( $\text{CH}_3\text{-(C=O)-CH}_3$ ) is developed, validated and then compared with four molecular models from the literature. The unlike dispersive interaction between nitrogen and acetone as well as oxygen and acetone is adjusted. Based on these mixture models, the VLE of nitrogen + acetone and oxygen + acetone is determined by molecular simulation and validated on the basis of experimental data. To extend the experimental database, a gas solubility apparatus is constructed and the saturated liquid line of nitrogen + acetone is measured at the three isotherms 400, 450 and 480 K up to a maximum pressure of 41 MPa. Finally, the results from simulation and experiment are used to parameterize the Peng-Robinson EOS for nitrogen + acetone with the Huron Vidal mixing rule.

**Keywords:** molecular model; experiment; vapor-liquid equilibrium; acetone; nitrogen; oxygen

---

\*corresponding author, tel.: +49-5251/60-2421, fax: +49-5251/60-3522,  
email: jadran.vrabec@upb.de

# 1 Introduction

Liquids, which are injected into a gaseous environment that has a supercritical state with respect to them, play an important role in energy conversion processes like Diesel and rocket engines or gas turbines. The challenge is to understand and model phenomena in transcritical jets, where liquids change their state after injection to a supercritical fluid. The Collaborative Research Center Transregio 75 "Droplet Dynamics Under Extreme Ambient Conditions" (SFB-TRR75),<sup>1,2</sup> which is funded by Deutsche Forschungsgemeinschaft (DFG), investigates the injection of acetone droplets into a nitrogen/oxygen environment by experiment and computational fluid dynamics simulation.<sup>3,4</sup> Knowledge on the phase behavior and other thermodynamic properties for these systems is crucial to undertake this task. In preceding work,<sup>5</sup> we measured the VLE of nitrogen + acetone and of oxygen + acetone below 400 K by experiment.

In this work, the VLE of the binary mixtures nitrogen + acetone and oxygen + acetone was studied by molecular simulation and additional experiments were carried out with a focus on the extended critical region of nitrogen + acetone. First, a force field model for acetone ( $\text{CH}_3\text{-(C=O)-CH}_3$ ), parameterized on the basis of quantum chemical calculations and experimental data for the saturated liquid density as well as the vapor pressure, was developed and compared with molecular models from the literature, i.e. the TraPPE model,<sup>6</sup> a modified version thereof,<sup>7</sup> the AUA4 model<sup>8</sup> and the OPLS model.<sup>9</sup> The present molecular acetone model was validated with the fundamental equation of state (EOS) by Lemmon and Span<sup>10</sup> and with experimental pure fluid data from the literature with respect to the heat of vaporization, various properties in the homogeneous fluid region (density, isobaric heat capacity, enthalpy, speed of sound), the second virial coefficient, the self-diffusion coefficient, the shear viscosity and the thermal conductivity.

Combining this acetone model with molecular models for nitrogen ( $\text{N}_2$ ) and for oxygen ( $\text{O}_2$ )

from prior work,<sup>11</sup> the unlike dispersive interaction between nitrogen and acetone as well as oxygen and acetone was adjusted. Based on these mixture models, the VLE of nitrogen + acetone and oxygen + acetone was determined by molecular simulation and assessed with the present experimental data. To this end, an apparatus was constructed to measure the saturated liquid line for nitrogen + acetone at the three isotherms 400, 450 and 480 K up to a maximum pressure of 41 MPa. For temperatures below 400 K and for oxygen + acetone, experimental data from prior work<sup>5</sup> were used.

In addition, for nitrogen + acetone the Peng-Robinson EOS was parameterized. The aim was to provide an EOS that yields reasonable results also near the critical line of the mixture for applications in the SFB-TRR75 as mentioned above. Parameters for the Huron Vidal mixing rule<sup>12</sup> were determined.

## 2 Experimental setup

### 2.1 Apparatus

The experimental setup for the present gas solubility measurements is shown in Fig. 1. Its main part was a cylindrical high pressure equilibrium cell made of V4a stainless steel, which has an internal volume of approximately 14 ml. A magnetic stirrer was placed into the cell. To visually observe phase separation inside, two sapphire gauge-glasses were mounted at the front and the back of the cylinder. The cell was constructed for pressures up to 70 MPa and temperatures up to 600 K. For this purpose, it was screwed together with eight expansion bolts and seven cup springs placed on each bolt. The cell was embedded in a copper cylinder with electrical heating. In this way, the temperature can be controlled effectively and automatically. To avoid heat loss due to radiation, the cell was surrounded by an aluminum cylinder with its own electrical heating. The whole setup was placed in a vacuum chamber to reduce heat loss

due to convection. Moreover, the vacuum atmosphere was useful to prohibit corrosion or ice formation at low temperatures.

The cell was loaded via a three-way valve mounted at the top. A gas bottle was connected to the left access (V1a) to load the gaseous component. The liquid component was loaded via a high pressure spindle press which was linked to the right access (V1b). The high pressure pump was connected to a liquid reservoir via valve V3. Valve V5 was used to purge the cell or to connect it to a vacuum pump. The pressure transducers P1 and P2 were used to measure the pressure of the gaseous and the liquid components in the supply pipes during the loading process. The pressure in the cell was determined with the pressure transducer P3, which was possible even if valve V4 was closed. The accuracy of all employed pressure transducers (model Super TJE, Honeywell test & measurement) was given as 0.1 % of their respective full measuring scale. The measuring scale was 20, 100 and 70 MPa for P1, P2 and P3, respectively. For the temperature measurement, five calibrated platinum resistance thermometers with a basic resistance of 100  $\Omega$  (Pt100) were installed in the apparatus. Thereby, the temperature of the fluid in the cell and in the high pressure pump were measured with the Pt100 thermometers T1 and T2, respectively. The temperature of the aluminum cylinder was determined with T4. The thermometers T3 and T5 were exclusively used to control the temperature of the cell and the aluminum cylinder, respectively. To calibrate the employed thermometers, a more precise platinum resistance thermometer with a basic resistance of 25  $\Omega$  was employed. The temperature measuring error was about  $\pm 0.04$  K.

## 2.2 Materials

Nitrogen 5.0 (volume fraction 0.99999) was obtained from Air Liquide. Acetone with a purity  $> 99.9$  % was purchased from Merck and degassed under vacuum.

### 2.3 Typical measuring procedure for the mixture nitrogen + acetone

Before loading the components of the studied mixture into the cell, the whole setup including the supply pipes was evacuated and thermostated close to the ambient temperature. Then, the gaseous component (nitrogen) was filled into the cell from the gas bottle. The density of nitrogen was calculated with the EOS by Span et al.<sup>13</sup> on the basis of the measured temperature and pressure. With the density from the EOS and the known cell volume, the mass of nitrogen  $m_{\text{N}_2}$  in the cell can be calculated. Next, the desired amount of the liquid component (acetone) was added into the cell with the calibrated spindle press. To achieve a homogeneous mixture, a magnetic stirrer was operated and the cell was heated up to a temperature that was about 20 K above the desired measuring temperature  $T_D$ . The mixing process was visually inspected with an endoscope and it was completed when all gas bubbles disappeared. At this point, the mixture was in a homogeneous state.

In a next step, the cell was slowly cooled down towards  $T_D$ , with the aim to reach the saturated liquid state in the vicinity of the temperature  $T_D$ . In this case, the measured pressure is the saturated vapor pressure of the mixture with a specified liquid composition at  $T_D$ . However, usually saturation precisely at  $T_D$  could not be reached with the present procedure. Therefore, several iterations were typically necessary, which are described in the following.

From a homogeneous fluid state, the cell was slowly cooled down towards the desired measuring temperature  $T_D$ . During this cooling process, the pressure of the mixture was measured with the pressure transducer P3 and plotted over time with the measurement program. At a certain temperature, the first small bubbles appeared and the slope of the pressure-time plot changed significantly. At this temperature, the mixture in the cell had reached the saturated liquid state. If the cell temperature was near  $T_D$ , the measured pressure was noted as the saturated vapor pressure of the mixture. Otherwise, if the cell temperature was significantly above  $T_D$  when the

bubbles appeared, the amount of acetone in the cell was too small. In this case, more acetone was added into the cell with the spindle press. This procedure, namely adding more acetone into the cell, raising the cell temperature by about 20 K, waiting for equilibration and then cooling it down until bubbles appeared, was repeated until the cell temperature was near the desired measuring temperature  $T_D$  when the mixture reached saturation.

In the last step, the mass of acetone  $m_{\text{Ace}}$  that was filled into the cell was determined as follows

$$m_{\text{Ace}} = \rho_1(T_1, p_1) \cdot V_1(z_1) - \rho_2(T_2, p_2) \cdot V_2(z_2), \quad (1)$$

wherein  $p$  is the pressure (measured with P3),  $T$  the temperature (measured with T4),  $\rho$  the pure acetone density calculated with the EOS by Lemmon and Span<sup>10</sup> and  $V$  the volume of the spindle press, which depends on its axial position  $z$ . The indices 1 and 2 represent before and after the filling process, respectively. Knowing the masses of nitrogen  $m_{\text{N}_2}$  and acetone  $m_{\text{Ace}}$ , the mole fraction  $x_{\text{N}_2}$  of the mixture can be determined straightforwardly.

## 3 Molecular models

### 3.1 Molecular models for the pure fluids

#### 3.1.1 Molecular model for acetone

In this work, a rigid and non-polarizable molecular model for acetone ( $\text{CH}_3\text{-(C=O)-CH}_3$ ) was developed, which considers the repulsive, dispersive and electrostatic interactions between the molecules. The repulsive and dispersive interactions were described by the Lennard-Jones (LJ) 12-6 potential and the electrostatic interactions by a point dipole and a point quadrupole. The total intermolecular interaction energy thus writes as

$$\begin{aligned}
U = & \sum_{i=1}^{N-1} \sum_{j=i+1}^N \left\{ \sum_{a=1}^{S_i^{\text{LJ}}} \sum_{b=1}^{S_j^{\text{LJ}}} 4\varepsilon_{ijab} \left[ \left( \frac{\sigma_{ijab}}{r_{ijab}} \right)^{12} - \left( \frac{\sigma_{ijab}}{r_{ijab}} \right)^6 \right] + \right. \\
& \left. \sum_{c=1}^{S_i^e} \sum_{d=1}^{S_j^e} \frac{1}{4\pi\epsilon_0} \left[ \frac{\mu_{ic}\mu_{jd}}{r_{ijcd}^3} \cdot f_1(\boldsymbol{\omega}_i, \boldsymbol{\omega}_j) + \frac{\mu_{ic}Q_{jd} + Q_{ic}\mu_{jd}}{r_{ijcd}^4} \cdot f_2(\boldsymbol{\omega}_i, \boldsymbol{\omega}_j) + \frac{Q_{ic}Q_{jd}}{r_{ijcd}^5} \cdot f_3(\boldsymbol{\omega}_i, \boldsymbol{\omega}_j) \right] \right\}, \quad (2)
\end{aligned}$$

where  $r_{ijab}$ ,  $\varepsilon_{ijab}$  and  $\sigma_{ijab}$  are the distance, the LJ energy parameter and the LJ size parameter, respectively, for the pair-wise interaction between LJ site  $a$  on molecule  $i$  and LJ site  $b$  on molecule  $j$ . The permittivity of vacuum is  $\epsilon_0$ , whereas  $\mu_{ic}$  and  $Q_{ic}$  denote the dipole moment and the quadrupole moment of the electrostatic interaction site  $c$  on molecule  $i$  and so forth. The expressions  $f_x(\boldsymbol{\omega}_i, \boldsymbol{\omega}_j)$  stand for the dependence of the electrostatic interactions on the orientations  $\boldsymbol{\omega}_i$  and  $\boldsymbol{\omega}_j$  of the molecules  $i$  and  $j$ .<sup>14,15</sup> Finally, the summation limits  $N$ ,  $S_x^{\text{LJ}}$  and  $S_x^e$  denote the number of molecules, the number of LJ sites and the number of electrostatic sites, respectively. Note that point dipoles or point quadrupoles can be replaced by two or three point charges,<sup>16</sup> respectively.

The present acetone model consists of four LJ sites. Two of these sites were located at the oxygen (O) and carbon (C) atoms. The others represent the two methyl (CH<sub>3</sub>) groups. Therein, the hydrogen atoms were only implicitly considered, following the united atom approach. The dipole was placed in the geometric center of the molecule and the quadrupole was located between the two CH<sub>3</sub> groups. The geometric structure of the molecule was determined by quantum chemical calculations using the software package GAMESS(US)<sup>17</sup> with the Hartree-Fock method and the 6-31G basis set. The magnitude and orientation of the dipole and quadrupole were subsequently specified according to the electron density distribution as obtained with the Møller-Plesset 2 method and the 6-311G(d,p) basis set. The positions of the atoms were taken from the preceding step for these calculations. The dipole and quadrupole magnitudes were estimated with the Mulliken approach.<sup>18</sup> The LJ parameters  $\sigma$  and  $\epsilon$  were initially adopted from

other similar models by Huang et al.<sup>19</sup> The model was optimized to experimental VLE data (saturated liquid density and vapor pressure) of pure acetone by varying the LJ parameters. In the last step, all model parameters, including those for geometry and polarity, were fine-tuned with the reduced unit method.<sup>20</sup> The parameters of the molecular acetone model are listed in Table 1.

It should be noted that the dipole moment magnitude of small molecules is larger in the liquid state than in the gaseous state due to increased mutual polarization. In the present molecular acetone model that was optimized primarily on the basis of properties of the liquid, this is reflected by a dipole moment magnitude that is approximately 20 % larger than its ideal gas phase value. Similar observations were made for numerous other molecular models.<sup>19,21</sup>

### **3.1.2 Molecular models for nitrogen and oxygen**

Molecular models for the pure fluids nitrogen and oxygen were needed for the studied binary mixtures nitrogen + acetone and oxygen + acetone. Models consisting of two LJ sites and one point quadrupole were developed for these components in prior work of our group<sup>11</sup> and were used here.

## **3.2 Molecular models for the binary mixtures nitrogen + acetone and oxygen + acetone**

To describe a binary mixture on the basis of pairwise additive potential models, two types of interactions between the molecules have to be specified. These are the interactions between like and between unlike molecules, where the like interactions are fully known from the pure substance models.

The unlike interactions can be separated into the electrostatic contribution and the repulsive/dispersive contribution. Unlike electrostatic interactions, e.g. between the acetone dipole

and the nitrogen quadrupole, are straightforwardly known from the laws of electrostatics. However, for the repulsive and dispersive interactions between the unlike molecules A and B, the LJ parameters  $\sigma_{AB}$  and  $\epsilon_{AB}$  have to be determined. This procedure was discussed by Schnabel et al.<sup>22</sup> in detail. The unlike LJ parameters can be written as

$$\sigma_{AB} = (\sigma_A + \sigma_B)/2, \tag{3}$$

and

$$\epsilon_{AB} = \xi \sqrt{\epsilon_A \cdot \epsilon_B}, \tag{4}$$

wherein  $\xi$  is a binary interaction parameter that can be adjusted to one experimental data point of the binary mixture. The vapor pressure of the mixture or the Henry’s law constant are good choices for this adjustment.<sup>23</sup> For the system nitrogen + acetone, the Henry’s law constant at 314.25 K as reported by Horiuti<sup>24</sup> and for oxygen + acetone the vapor pressure at 283.15 K and  $x_{O_2} = 0.005$  mol/mol, which was measured in preceding work,<sup>5</sup> were used for the adjustment. The optimized values are  $\xi = 0.96$  for nitrogen + acetone and  $\xi = 0.905$  for oxygen + acetone.

## 4 Results and discussion

### 4.1 Simulation results for pure acetone

In the following sections, the simulation results for the VLE behavior, different thermodynamic properties in the homogeneous region, the second virial coefficient and transport properties in the liquid state on the basis of the present acetone model are compared with experimental data and with the EOS by Lemmon and Span,<sup>10</sup> which is recommended by the National Institute for Standards and Technology (NIST), or with correlations from the DIPPR database.<sup>25</sup> In case of VLE, the present acetone model was also compared with the TraPPE model by Stubbs et al.,<sup>6</sup> a

modified version thereof by Kamath et al.,<sup>7</sup> the AUA4 model by Ferrando et al.<sup>8</sup> and the OPLS model by Jorgensen et al.<sup>9</sup> All present data from experiment and simulation are available in numerical form in the supplementary material. Simulation details are given in the appendix.

#### 4.1.1 VLE data

With respect to the VLE behavior and the properties in the homogeneous fluid region, the EOS by Lemmon and Span<sup>10</sup> was used as a reference. The stated uncertainties of the EOS are 0.1% for the saturated liquid density between 280 and 310 K, 0.5% for the density of the liquid phase below 380 K and 1% elsewhere. The uncertainties for the vapor pressure are 0.5% above 270 K and 0.25% between 290 and 390 K. In addition, experimental data compiled in the Dortmund Data Bank<sup>26</sup> and the DIPPR database<sup>25</sup> are shown as well.

Figs. 2 to 4 illustrate the saturated densities, the vapor pressure and the enthalpy of vaporization of acetone that were obtained with the present molecular model, the TraPPE model,<sup>6</sup> its modification,<sup>7</sup> the AUA4 model<sup>8</sup> and the OPLS model.<sup>9</sup> The relative deviations of all five models from the reference EOS<sup>10</sup> are plotted in Fig. 5. As can be seen, the present molecular model yields the best agreement with the reference EOS for all shown properties. Only for the saturated liquid density at temperatures above about 400 K, the modified TraPPE model<sup>7</sup> exhibits smaller deviations.

The critical values for temperature, density and pressure were calculated on the basis of the present simulation data with a method suggested by Lotfi et al.<sup>27</sup> The critical values for the present model  $T_c = 509.2$  (508.1) K,  $\rho_c = 4.78$  (4.7) mol/l and  $p_c = 4.72$  (4.7) MPa agree well with the results of the reference EOS<sup>10</sup> (values in parentheses). The agreement is within the estimated uncertainties of the present simulation data, being 0.5 % for  $T_c$ , 2 % for  $\rho_c$  and 4 % for  $p_c$ . The critical properties from the reference EOS, the present molecular model and the four models from the literature are summarized in Table 2.

### 4.1.2 Homogeneous region

In the homogeneous region, simulations were carried out for density, isobaric heat capacity, speed of sound and residual enthalpy over a temperature range from 200 to 550 K and a pressure range from 5 to 95 MPa. The uncertainties of the reference EOS<sup>10</sup> for the isobaric heat capacity and the speed of sound are 1%. However, its uncertainties for these properties may be higher at pressures above the saturation pressure and at temperatures above 320 K in the liquid phase and under supercritical conditions.<sup>10</sup>

The isobaric heat capacity  $c_p$  was calculated here as a sum of the residual and the ideal gas contribution

$$c_p = c_p^{res} + c_p^{id}, \quad (5)$$

wherein the residual contribution  $c_p^{res}$  was obtained from molecular simulation and the ideal gas contribution was taken from the reference EOS.<sup>10</sup> For the enthalpy, only the residual contribution  $h^{res} = h - h^{id}$  was used for comparison. The speed of sound  $c$  can be calculated as

$$c = \frac{1}{\sqrt{M\beta\rho - T\alpha^2/c_p^{id}}}, \quad (6)$$

where  $M$  is the molar mass,  $\beta$  the isothermal compressibility,  $\rho$  the density and  $\alpha$  the volume expansivity. Except for  $c_p^{id}$ , all data on the right hand side of Eq. (6) were obtained directly by molecular simulation.

The relative deviations of the simulation data from the reference EOS<sup>10</sup> are mainly below 1 % for the density as well as for the isobaric heat capacity and below 2 % for the speed of sound as well as for the residual enthalpy over the entire temperature and pressure range. Only near the critical point, the deviations may be significantly larger, cf. Fig. 6.

### 4.1.3 Second virial coefficient

The second virial coefficient was predicted over a temperature range from 240 to 2500 K by evaluating Mayer's  $f$ -function. This approach was described e.g. by Huang et al.<sup>19</sup> Fig. 7 shows the results in comparison to experimental data and a correlation from the DIPPR database.<sup>25</sup> Over the whole temperature range, the present data are in excellent agreement with the experimental data. The average absolute deviation to the correlation in a temperature range from 400 to 2500 K is only 6.4 ml/mol.

### 4.1.4 Transport properties

Transport properties of liquid acetone were obtained by equilibrium molecular dynamics (EMD) simulations following the Green-Kubo formalism, cf. Guevara-Carrion et al.<sup>28</sup> Figs. 8 to 10 illustrate the simulation results for self-diffusion coefficient, shear viscosity and thermal conductivity along the saturated liquid line from 190 to 325 K in comparison with experimental data and correlations. In case of the self-diffusion coefficient, the correlation was published by Ertl and Dullien.<sup>29</sup> Correlations from the DIPPR database<sup>25</sup> were used for the shear viscosity and the thermal conductivity. For all considered transport properties, the simulation data agree very well with the experiment and the correlations over the entire temperature range. The mean deviations between the simulation points and the correlations is 8 %, 7 % and 9 % for self-diffusion coefficient, shear viscosity and thermal conductivity, respectively. Transport properties were not considered in the parameterization of the molecular model.

## 4.2 Simulation results for nitrogen + acetone and oxygen + acetone at low temperatures

VLE data of the binary mixtures nitrogen + acetone and of oxygen + acetone were measured experimentally and compared to the available experimental data from the literature in a preceding publication.<sup>5</sup> In that work,<sup>5</sup> the saturated liquid line for nitrogen + acetone was determined for eight isotherms between 223 and 400 K up to a pressure of 12 MPa. For oxygen + acetone, two isotherms at 253 and 283 K up to a pressure of 0.75 MPa were measured. Based on these data, the Henry's law constant was calculated. In addition, the saturated vapor line of nitrogen + acetone was studied for three isotherms between 303 and 343 K up to a pressure of 1.8 MPa. In the following, the simulation results for nitrogen + acetone and oxygen + acetone, which are based on the molecular mixture models from present work, are assessed on the basis of the data discussed above.<sup>5</sup>

### 4.2.1 Nitrogen + acetone

The simulation results for the saturated liquid line and the saturated vapor line of nitrogen + acetone are shown in Figs. 11 and 12, respectively. For the saturated liquid line, eight isotherms between 223.15 and 400 K up to a pressure of 11 MPa were simulated. For the saturated vapor line, simulations were carried out for the three isotherms 303.15, 323.15 and 343.15 K up to a pressure of 2 MPa. The experimental data points and the Peng-Robinson EOS with the Huron-Vidal mixing rule from prior work<sup>5</sup> are plotted in Figs. 11 and 12 as well. For both the saturated liquid line and the saturated vapor line, the simulation results agree well with the experimental data and the Peng-Robinson EOS. The mean deviation between all simulation points and the Peng-Robinson EOS with respect to the vapor pressure is less than 2 % for the saturated liquid line and less than 0.15 MPa for the saturated vapor line. In terms of the mole fraction, nearly

all simulation points agree with the Peng-Robinson EOS within their statistical uncertainties. For the Henry’s law constant of nitrogen + acetone, simulations were carried out between 225 and 470 K, cf. Fig. 13. Simulation details are given in the appendix. As described in section 3.2, the molecular mixture model was adjusted to the Henry’s law constant  $H = 176.4 \text{ MPa}^{24}$  at 314.25 K. Compared to the Henry’s law constant from our preceding work<sup>5</sup> and other literature,<sup>24,30,47–51</sup> the present simulations are in good line with the experimental data. The mean deviation between the simulation points and the straight line in Fig. 13 is only 1.3 %.

#### 4.2.2 Oxygen + acetone

In Fig. 14, the present simulation results for the saturated liquid line of oxygen + acetone at 253.15 and 283.15 K are compared with experimental data and the Peng-Robinson EOS.<sup>5</sup> Note that the plotted region for the pressure and the mole fraction is quite small, the maximum pressure is 0.8 MPa and the maximum oxygen mole fraction is only about 0.006 mol/mol. It can be seen that the points that belong to the 253.15 K isotherm do not differ much from the points that belong to the 283.15 K isotherm. Obviously, this is due to the intersection of both saturated liquid lines at a mole fraction  $\approx 0.0015 \text{ mol/mol}$ . Fig. 14 shows good agreement between simulation, experiment and the Peng-Robinson EOS. The mean deviation of the simulated vapor pressure and that obtained from the Peng-Robinson EOS is 2.2 %.

Simulations for the Henry’s law constant of oxygen in acetone were carried out in a temperature range between 243.15 and 293.15 K, cf. Fig. 13. The predicted values agree with the experimental Henry’s law constant<sup>5</sup> almost within their statistical simulation uncertainties. Overall, the simulation points lie approximately in the center of the experimental data from the literature and follow the temperature dependence e.g. by Horiuti<sup>24</sup> or by Kretschmer et al.<sup>30</sup>

### 4.3 Results for the VLE behavior of nitrogen + acetone in the transcritical region

Due to the lack of experimental data at high pressures in the literature, measurements with the apparatus introduced in section 2.1 and simulations with the molecular model discussed in section 3.2 were carried out for nitrogen + acetone for the three isotherms 400, 450 and 480 K ( $\pm 5$  K for the experimental measurements). These data points are shown in Figs. 15 to 17. It can be seen that the simulation data and the data from experiment agree well in the region of small mole fractions  $x_{\text{N}_2}$  for all three isotherms. However, with rising  $x_{\text{N}_2}$ , particularly in the near critical region, the molecular model overestimates the vapor pressure of the mixture.

## 5 Peng-Robinson equation of state

To correlate the experimental data generated in the present work, the Peng-Robinson EOS<sup>31</sup> was used

$$p = \frac{RT}{v - b} - \frac{a}{v \cdot (v + b) + b \cdot (v - b)}. \quad (7)$$

The substance specific parameters  $a$  and  $b$  were defined as

$$a = \left(0.45724 \cdot \frac{R^2 T_c^2}{p_c}\right) \cdot [1 + (0.37464 + 1.54226 \cdot \omega - 0.26992 \cdot \omega^2) \cdot (1 - \sqrt{\frac{T}{T_c}})]^2, \quad (8)$$

and

$$b = 0.07780 \cdot \frac{RT_c}{p_c}. \quad (9)$$

Therein,  $R$  is the ideal gas constant,  $v$  the molar volume,  $T_c$  the critical temperature,  $p_c$  the critical pressure and  $\omega$  the acentric factor, cf. Tab. 3.

To describe mixtures with the Peng-Robinson EOS, numerous mixing rules can be found in the literature. For nitrogen + acetone and oxygen + acetone at low temperatures and far away from

the critical region of the mixture, the quadratic mixing rule<sup>32</sup> and the Huron-Vidal<sup>12</sup> mixing rule combined with the UNIQUAC  $g^E$  model were adjusted in prior work.<sup>5</sup>

The Huron-Vidal mixing rule states that the pure substance parameters  $a$  and  $b$  have to be replaced by

$$a_m = b_m \left( \sum_i \frac{a_i}{b_i} x_i - \frac{g_\infty^E}{\Lambda} \right), \quad (10)$$

where

$$\Lambda = \frac{1}{2\sqrt{2}} \cdot \ln \left( \frac{2 + \sqrt{2}}{2 - \sqrt{2}} \right), \quad (11)$$

and

$$b_m = \sum_i x_i b_i, \quad (12)$$

if the Peng-Robinson EOS is used. The excess Gibbs free energy at infinite pressure  $g_\infty^E$  can be calculated with an appropriate  $g^E$  model. In the present work, the UNIQUAC model<sup>33</sup> was used for this task, which requires the two binary interaction parameters  $l_{ij}$  and  $l_{ji}$ .

However, the present experimental and simulation results for nitrogen + acetone show that both parameterizations of the Peng-Robinson EOS that we published in prior work<sup>5</sup> yield poor results for the 400, 450 and 480 K isotherms. In Ref.,<sup>5</sup> the binary parameters for the Huron-Vidal mixing rule were specified to be  $l_{ji} = 241.9$  and  $l_{ij} = 926.5$ . To achieve better results in the near-critical region, the Peng-Robinson EOS was readjusted to the present data at 480 K, considering the parameterization from Ref.<sup>5</sup> The binary parameters of the Huron-Vidal mixing rule were assumed to be temperature-dependent with

$$l_{ij} = \begin{cases} 241.9 & \text{for } 223 \leq T / \text{K} \leq 400, \text{ cf. Ref.}^5 \\ -12.24 \cdot T/\text{K} + 5136 & \text{for } 400 < T / \text{K} \leq 480, \end{cases} \quad (13)$$

and

$$l_{ji} = \begin{cases} 926.5 & \text{for } 223 \leq T / \text{K} \leq 400, \text{ cf. Ref.}^5 \\ 25.47 \cdot T/\text{K} - 9261 & \text{for } 400 < T / \text{K} \leq 480. \end{cases} \quad (14)$$

The binary parameters are continuous at 400 K.

The Peng-Robinson EOS using the Huron-Vidal mixing rule is shown in Figs. 15 to 17 for the isotherms 400, 450 and 480 K. There is reasonable agreement with experiment and simulation in the extended critical region.

The parameterization of the Peng-Robinson EOS using the quadratic mixing rule shows that this mixing rule does not yield reasonable results in a wide temperature and composition range. The correlation of the present data between 400 and 480 K leads to a temperature-dependent binary parameter of the quadratic mixing rule of  $k_{ij} = -0.0026 \cdot T/\text{K} + 1.237$ .

## 6 Conclusion

VLE of the systems nitrogen + acetone and oxygen + acetone were studied by molecular simulation. In addition, experiments were carried out for nitrogen + acetone. A new force field model for acetone was developed and validated with the EOS by Lemmon and Span<sup>10</sup> as well as with various experimental data from the literature. It was shown that there is a good agreement between simulation, the EOS and the experimental literature data throughout. For a large part of the homogeneous fluid state, the deviations are mainly below 1 % for the density and isobaric heat capacity and below 2 % for the speed of sound and the residual enthalpy. The average difference between simulation and EOS for the second virial coefficient was found to

be only 6.4 ml/mol over a wide temperature range. For the self-diffusion coefficient, the shear viscosity and the thermal conductivity in a range of liquid states, the mean deviation between simulation and correlations of experimental data was smaller than 9 %. In addition, the present model was compared to four molecular models from the literature in terms of saturated liquid density, vapor pressure and heat of vaporization. Almost throughout, the present model yields the smallest deviations with respect to the reference EOS.

For nitrogen + acetone and oxygen + acetone, the binary parameter  $\xi$  for the unlike dispersive interaction was adjusted to one experimental data point of each mixture. Subsequently, simulations were carried out to predict the VLE of these two systems. For nitrogen + acetone at 400, 450 and 480 K up to a pressure of 41 MPa, the simulation results were validated with data points for the saturated liquid line measured in this work by means of a newly constructed experimental setup. For lower temperatures and for oxygen + acetone, experimental data from preceding work<sup>5</sup> were used for validation. It was shown that the agreement between simulation and experiment is good for oxygen + acetone and for nitrogen + acetone for temperatures below 400 K. Above 400 K and at high pressures, the simulation points were above the experimentally measured points. Based on the obtained data for nitrogen + acetone the Peng-Robinson EOS using the Huron-Vidal mixing rule was parameterized.

## Acknowledgment

This work was funded by Deutsche Forschungsgemeinschaft, Collaborative Research Center Transregio 75 "Droplet Dynamics Under Extreme Ambient Conditions" and project grant VR6/9-1. Furthermore, the authors wish to thank Elmar Baumhögger for his support in the experimental investigations, Gabriela Guevara-Carrion for her valuable suggestions with respect to transport data as well as Christoph Klink for fruitful discussions.

## Supporting Information

Tables S1 to S8. This material is available free of charge via the Internet at <http://pubs.acs.org>.

## 7 Appendix: Simulation details

In this work, the Grand Equilibrium method<sup>34</sup> was used for the VLE calculations of pure acetone. To determine the chemical potential in the liquid, Widom's test molecule method<sup>35</sup> was applied. For this task, molecular dynamics (MD) simulations containing 864 molecules were carried out. Starting from a face-centered cubic lattice, 150 000 time steps were sampled for equilibration with the first 50 000 time steps in the canonical ( $NVT$ ) ensemble. The production run was performed for 1 000 000 steps. The time step was set to 2 fs and the Gear-predictor corrector integrator was used. The chemical potential was determined by inserting 3456 test molecules every time step into the simulation volume and averaging over all results. For the corresponding vapor, the simulation volume was adjusted to lead to an average number of 500 molecules. After 5 000 initial  $NVT$  Monte Carlo (MC) cycles, starting from a face centered cubic lattice, 5 000 equilibration cycles in the pseudo- $\mu VT$  ensemble were carried out. The length of the production run was 200 000 cycles. For the mixture oxygen + acetone and for nitrogen + acetone below 400 K, the same settings as described above were used for both the

liquid and the vapor simulations. For the VLE of nitrogen + acetone at isotherms above 400 K, the  $NpT$ +test particle method<sup>36</sup> in an extended version was used. On the liquid side, one MC  $NpT$  simulation and one MC  $NVT$  simulation were carried out. The  $NpT$  simulation at a specified pressure yielded the partial molar volumes, the  $NVT$  simulation at the density obtained from the  $NpT$  run supplied the chemical potential. For the corresponding vapor, two MC  $NpT$  simulations and two MC  $NVT$  simulations at slightly different composition were performed at the specified pressure. Again, the  $NpT$  simulations yielded the partial molar volumes. The chemical potentials were obtained from the  $NVT$  simulations. Using these data, the VLE at a given temperature  $T$  and liquid composition  $x$  was calculated.

For the homogeneous properties of pure acetone, MC simulations in the  $NpT$  ensemble were carried out with 864 molecules. Again, starting from a face-centered cubic lattice, 30 000 MC cycles were sampled for equilibration with the first 10 000 cycles in the  $NVT$  ensemble. The production run was performed for 200 000 cycles.

Transport properties were determined by equilibrium MD simulations following the Green-Kubo formalism.<sup>37,38</sup> For that task, MD simulations were carried out in two steps. In the first step, one simulation in the  $NpT$  ensemble was carried out at the specified temperature and pressure to obtain the density. The system was equilibrated over 100 000 time steps, thereof 50 000 in the  $NVT$  ensemble, followed by a production run of 500 000 time steps. In the second step, a  $NVT$  ensemble simulation was performed at this temperature and density to calculate the transport properties. The simulations were equilibrated in the  $NVT$  ensemble over 200 000 time steps, followed by production runs of 3 500 000 to 7 000 000 time steps. The simulation length was chosen to obtain at least 20 000 independent time origins of the autocorrelation functions. The sampling length of the autocorrelation functions was chosen to be between 6

und 24 ps, depending on the long-time behavior of the shear viscosity autocorrelation function. The separation between the time origins was chosen such that all autocorrelation functions had decayed at least to  $1/e$  of their normalized value to guarantee their time independence.<sup>39</sup>

To calculate the Henry’s law constant, the residual chemical potential of the gaseous component  $i$  at infinite dilution in the liquid  $\mu_i^\infty$  was evaluated using Widom’s test molecule method. The mole fraction of the solute in the solvent was exactly zero, as required for infinite dilution. MD simulations were carried out in the liquid state at a specified temperature and the pressure was set to the pure substance vapor pressure of the solvent, as described by the molecular model. Therefore, test molecules representing the solute  $i$  were inserted into the pure saturated liquid solvent after each time step at random spatial coordinates and orientations and the potential energy  $\psi_i$  between the solute test molecule  $i$  and all solvent molecules was calculated. Thus only solute-solvent interactions were sampled. The number of test molecules was 3456 every time step. The residual chemical potential at infinite dilution  $\mu_i^\infty$  was then obtained by

$$\mu_i^\infty = -k_B T \ln \langle V \exp(-\psi_i/(k_B T)) \rangle / \langle V \rangle, \quad (15)$$

where  $V$  is the volume and the brackets represent the  $NpT$  ensemble average.

All thermodynamic properties were determined in the production phase of the simulations on the fly. The cut-off radius was set to 17.5 Å throughout and a center of mass cut-off scheme was applied. Lennard-Jones long-range interactions beyond the cut-off radius were corrected employing angle averaging as proposed by Lustig.<sup>40</sup> Electrostatic interactions were corrected with the reaction field method.<sup>14</sup> The statistical uncertainties of all results were estimated by block averaging according to Flyvbjerg and Petersen<sup>41</sup> and the error propagation law.

## References

- (1) <http://www.sfbtrr75.de/website/index.php>.
- (2) Weigand, B.; Tropea, C. Droplet dynamics under extreme boundary conditions: The collaborative research center SFB-TRR 75. *ICLASS* **2012**.
- (3) Oldenhof, E.; Weckenmann, F.; Lamanna, G.; Weigand, B.; Bork, B.; Dreizler, A. Experimental Investigation of Isolated Acetone Droplets at Ambient and Near-Critical Conditions, injected in a nitrogen atmosphere. *Progress in Propulsion Physics* **2013**, 4, 257-270.
- (4) Chrigui, M.; Gounder, J.; Sadiki, A.; Masri, A.; Janicka, J.: Partially premixed reacting acetone spray using LES and FGM tabulated chemistry. *Combustion and Flame* **2012**, 159, 2718-2741.
- (5) Windmann, T.; Köster, A.; Vrabec, J. Vapor-liquid equilibrium measurements of the binary mixtures nitrogen + acetone and oxygen + acetone. *J. Chem. Eng. Data* **2012**, 57, 1672-1677.
- (6) Stubbs, J.M.; Potoff, J.J.; Siepmann, J.I. Transferable Potentials for Phase Equilibria. 6. United-Atom Description for Ethers, Glycols, Ketones, and Aldehydes. *J. Phys. Chem. B* **2004**, 108, 17596-17605.
- (7) Kamath, G.; Georgiev, G.; Potoff, J.J. Molecular Modeling of Phase Behavior and Microstructure of Acetone-Chloroform-Methanol Binary Mixtures. *J. Phys. Chem. B* **2005**, 109, 19463-19473.
- (8) Ferrando, N.; Lachet, V.; Boutin, A. Monte Carlo Simulations of Mixtures Involving Ketones and Aldehydes by a Direct Bubble Pressure Calculation. *J. Phys. Chem. B* **2010**, 114, 8680-8688.

- (9) Jorgensen, W.L.; Madura, J.D.; Swenson, C.J. Optimized intermolecular potential functions for liquid hydrocarbons. *J. Am. Chem. Soc.* **1984**, 106, 6638.
- (10) Lemmon, E.W.; Span, R. Short Fundamental Equations of State for 20 Industrial Fluids. *J. Chem. Eng. Data* **2006**, 51, 785-850.
- (11) Vrabec, J.; Stoll, J.; Hasse, H. A Set of Molecular Models for Symmetric Quadrupolar Fluids. *J. Phys. Chem. B* **2001**, 105, 12126-12133.
- (12) Huron, M.J.; Vidal, J. New Mixing Rules in Simple Equations of State for Representing Vapour-Liquid Equilibria of Strongly Non-Ideal Mixtures. *Fluid Phase Equilib.* **1979**, 3, 255-271.
- (13) Span, R.; Lemmon, E.W.; Jacobsen, R.T.; Wagner, W.; Yokozeki, A. A Reference Equation of State for the Thermodynamic Properties of Nitrogen for Temperatures from 63.151 to 1000 K and Pressures to 2200 MPa. *J. Phys. Chem. Ref. Data* **2000**, 29, 1361-1433.
- (14) Allen, M.P.; Tildesley, D.J. Computer simulations of liquids. *Oxford University Press*, Oxford, 1987.
- (15) Gray, C.G.; Gubbins, K.E. Theory of molecular fluids. 1. Fundamentals. *Clarendon Press*, Oxford, 1984.
- (16) Engin, C.; Vrabec, J.; Hasse, H. On the difference between a point multipole and an equivalent linear arrangement of point charges in force field models for vapor-liquid equilibria. Partial charge based models for 59 real fluids. *Mol. Phys.* **2011**, 109, 1975-1982.
- (17) Schmidt, M.W.; Baldrige, K.K.; Boatz, J.A.; Elbert, S.T.; Gordon, M.S.; Jensen, J.H.; Koseki, S.; Matsunaga, N.; Nguyen, K.A.; Windus, T.L.; Dupuis, M.; Montgomery Jr.,

- J.A. General Atomic and Molecular Electronic Structure System. *J. Comput. Chem.* **1993**, 14, 1347-1363.
- (18) Mulliken, R.S. Criteria for the Construction of Good SelfConsistentField Molecular Orbital Wave Functions, and the Significance of LCAOMO Population Analysis. *J. Chem. Phys.* **1964**, 36, 3428-3440.
- (19) Huang, Y.-L.; Heilig, M.; Hasse, H.; Vrabec, J. Vapor-Liquid Equilibria of Hydrogen Chloride, Phosgene, Benzene, Chlorobenzene, Ortho-Dichlorobenzene and Toluene by Molecular Simulation. *AIChE J.* **2011**, 52, 1043-1060.
- (20) Stoll, J. Molecular Models for the Prediction of Thermalphysical Properties of Pure Fluids and Mixtures. *Fortschritt-Berichte VDI, Reihe 3, vol. 836*, VDI-Verlag, Düsseldorf, **2005**.
- (21) Eckl, B.; Vrabec, J.; Hasse, H. On the Application of Force Fields for Predicting a Wide Variety of Properties: Ethylene Oxide as an Example. *Fluid Phase Equilib.* **2008**, 274, 16-26.
- (22) Schnabel, T.; Vrabec, J.; Hasse, H. Unlike Lennard-Jones Parameters for Vapor-Liquid Equilibria. *J. Mol. Liq.* **2007**, 135, 170-178.
- (23) Schnabel, T.; Vrabec, J.; Hasse, H. Molecular simulation study of hydrogen bonding mixtures and molecular models for mono- and dimethylamine. *Fluid Phase Equilib.* **2008**, 263, 144-159.
- (24) Horiuti, J. On the solubility of gas; coefficient of dilatation by absorption. *Sci. Papers Inst. Phys. Chem. Res.(Japan)* **1931**, 17, 125-256.

- (25) Rowley, R.L.; Wilding, W.V.; Oscarson, J.L.; Yang, Y.; Zundel, N.A.; Daubert, T.E.; Danner, R.P. The DIPPR Data Compilation of Pure Compound Properties. Design Institute for Physical Properties, *AIChE*, New York, 2006.
- (26) Dortmund Data Bank, Mixture Properties, Version 6.3.0.384, 2010.
- (27) Lotfi, A.; Vrabec, J.; Fischer, J. Vapour liquid equilibria of the Lennard-Jones fluid from the NpT plus test particle method. *Mol. Phys.* **1992**, 76, 1319-1333.
- (28) Guevara-Carrion, G.; Nieto-Dracchi, C.; Vrabec, J.; Hasse, H. Prediction of Transport Properties by Molecular Simulation: Methanol and Ethanol and Their Mixture. *J. Phys. Chem. B* **2008**, 112, 16664-16674.
- (29) Ertl, H.; Dullien, F.A.L. Self-Diffusion and Viscosity of Some Liquids as a Function of Temperature. *AIChE J.* **1973**, 19, 1215-1223.
- (30) Kretschmer, C.B.; Nowakowska J.; Wiebe R. Solubility of oxygen and nitrogen in organic solvents from -25 to 50 C. *Ind. Eng. Chem.* **1946**, 38, 506-509.
- (31) Peng, D.Y.; Robinson, D.B. A New Two-Constant Equation of State. *Ind. Chem. Eng. Fundam.* **1976**, 15, 59-64.
- (32) Smith, J.M.; VanNess, H.C.; Abbott, M.M. *Introduction to chemical engineering*. McGraw-Hill, New York, 1996.
- (33) Abrams, D.; Prausnitz, J.M. Statistical thermodynamics of liquid mixtures: A new expression for the excess Gibbs energy of partly or completely miscible systems. *AIChE J.* **1975**, 21, 116-128.
- (34) Vrabec, J.; Hasse, H. Grand Equilibrium: vapour-liquid equilibria by a new molecular simulation method. *Mol. Phys.* **2002**, 100, 3375-3383.

- (35) Widom, B. Some Topics in the Theory of Fluids. *J. Chem. Phys.* **1963**, 39, 2808-2812.
- (36) Vrabec, J.; Fischer, J. Vapour liquid equilibria of mixtures from the NpT plus test particle method. *Mol. Phys.* **1995**, 85, 781-792.
- (37) Green, M.S. Markoff Random Processes and the Statistical Mechanics of Time-Dependent Phenomena. II. Irreversible Processes in Fluids. *J. Chem. Phys.* **1954**, 22, 398-413.
- (38) Kubo, R. Statistical-Mechanical Theory of Irreversible Processes. I. General Theory and Simple Applications to Magnetic and Conduction Problems. *J. Phys. Soc. Jpn.* **1957**, 12, 570-586.
- (39) Schoen, M.; Hoheisel, C. The mutual diffusion coefficient  $D_{12}$  in binary liquid model mixtures. Molecular dynamics calculations based on Lennard-Jones (12-6) potentials. *Mol. Phys.* **1984**, 52, 33-56.
- (40) Lustig, R. Angle-average for the powers of the distance between two separated vectors. *Mol. Phys.* **1988**, 65, 175-179.
- (41) Flyvbjerg, H.; Petersen, H.G. Error estimates on averages of correlated data. *J. Chem. Phys.* **1989**, 91, 461466.
- (42) McCall, D.W.; Douglass, D.C.; Anderson, E.W. Diffusion in Liquids. *J. Chem. Phys.* **1959**, 31, 1555-1557.
- (43) Krüger, G.J.; Weiss, R. Diffusionskonstanten einiger organischer Flüssigkeiten. *Z. Naturforsch.* **1979**, 25a, 777-780.
- (44) Holz, M.; Mao, X.; Seiferling, D.; Sacco, A. Experimental study of dynamic isotope effects in molecular liquids: Detection of translationrotation coupling. *J. Chem. Phys.* **1996**, 104, 669-679.

- (45) Wheeler, D.R.; Rowley, R.L. Shear viscosity of polar liquid mixtures via non-equilibrium molecular dynamics: water, methanol, and acetone. *Mol. Phys.* **1998**, *94*, 555-564.
- (46) Wohlfarth, C.; Wohlfahrt, B. M.D. Lechner (ed.), C3, SpringerMaterials - The Landolt-Börnstein Database, DOI: 10.1007/10639283\_4, 2013.
- (47) Jabloniec, A.; Horstmann, S.; Gmehling, J. Experimental Determination and Calculation of Gas Solubility Data for Nitrogen in Different Solvents. *Ind. Eng. Chem. Res.* **2007**, *46*, 4654-4659.
- (48) Just, G. Löslichkeit von Gasen in organischen Lösungsmitteln. *Z. Phys. Chem.* **1901**, *37*, 342-367.
- (49) Nitta, T.; Nakamura, Y.; Ariyasu, H.; Katayam, T. Solubilities of nitrogen in binary solutions of acetone with cyclohexane, benzene, chloroform and 2-propanol. *J. Chem. Eng. (Japan)* **1980**, *13*, 97-103.
- (50) Vosmansky, J.; Dohnal, V. Gas solubility measurements with an apparatus of the Ben-Naim-Baer type. *Fluid Phase Equilib.* **1987**, *33*, 137-155.
- (51) Tsuji, K.; Ichikawa, K.; Yamamoto, H.; Tokunaga, J. Solubilities of Oxygen and Nitrogen in Acetone-Water Mixed Solvent. *Kagaku Kogaku Ronbunshu* **1987**, *13*, 825-830.
- (52) Levi, M.G. Sull'energia basica dell' ossido di nrgento in soluzione. *Gazz. Chim. Ital.* **1901**, *31*, 513-541.
- (53) Fischer, F.; Pfeleiderer, G. Über die Löslichkeit von Sauerstoff in verschiedenen organischen Lösungsmitteln. *Z. Anorg. Allg. Chem.* **1922**, *124*, 61-69.
- (54) Finlayson, T.C. Industrial oxygen. *Trans. Inst. Chem. Engr.* **1923**, *1*, 3-83.

- (55) Schlaepfer, P.; Audykowski, T.; Bukowiecki, A. Über die Lösungsgeschwindigkeit des Sauerstoffs in verschiedenen Flüssigkeiten. *Schweizer Archiv für Wiss. u. Technik* **1949**, 15, 299-307.
- (56) Sinn, E.; Matthes, K.; Naumann, E. Experimentelle Untersuchungen über die Löslichkeit von Sauerstoff in flüssigen organischen Substanzen. *Wiss. Z. Fr.-Schiller-Univ. Jena, Math.-Naturwiss. R.* **1967**, 16, 523-529.
- (57) Naumenko, N.K. *Investigation on the Solubility of Oxygen in Organic Solvents*. PhD Thesis, Leningrad, 1970.
- (58) Bub, G.K.; Hillebrand, W.A. Solubility of oxygen in 2-propanone, 2-butanone, 2-pentanone; 2-hexanone. *J. Chem. Eng. Data* **1979**, 24, 315-319.
- (59) Luehring, P.; Schumpe, A. Gas Solubilities (H<sub>2</sub>, He, N<sub>2</sub>, CO, O<sub>2</sub>, Ar, CO<sub>2</sub>) in Organic Liquids at 293.2K. *J. Chem. Eng. Data* **1989**, 34, 250-252.

Table 1: Parameters of the present molecular model for acetone.  $x$ ,  $y$  and  $z$  are the coordinates with respect to the  $x$ ,  $y$  and  $z$  axis,  $\sigma$  and  $\epsilon$  are the Lennard-Jones size and energy parameter,  $\mu$  and  $Q$  are the dipole and quadrupole moment magnitudes. Lennard-Jones interaction sites are denoted by the modeled atoms or atomic groups. Electrostatic interaction sites are denoted by dipole or quadrupole, respectively. Coordinates are given with respect to the center of mass in a principal axes system. Orientations of the electrostatic sites are defined in standard Euler angles, where  $\varphi$  is the azimuthal angle with respect to the  $x - z$  plane and  $\theta$  is the inclination angle with respect to the  $z$  axis.

interaction site	$x$ Å	$y$ Å	$z$ Å	$\sigma$ Å	$\epsilon/k_B$ K	$\theta$ deg	$\varphi$ deg	$\mu^a$ $10^{-30}$ Cm	$\mu^a$ D	$Q^a$ $10^{-40}$ Cm <sup>2</sup>	$Q^a$ DÅ
C	0	0	0	2.9307	9.8216						
O	0	1.2095	0	3.3704	106.9873						
CH <sub>3</sub>	0	-0.8031	1.2853	3.6225	111.9795						
CH <sub>3</sub>	0	-0.8031	-1.2853	3.6225	111.9795						
dipole	0	0	0			90	90	11.4906	3.4448		
quadrupole	0	-0.8031	0			90	90			2.4377	0.7308

<sup>a</sup> Note that the magnitudes of the dipole and the quadrupole are given in SI units (left) and in Debye (right column).

Table 2: Critical temperature  $T_c$ , critical density  $\rho_c$  and critical pressure  $p_c$  of pure acetone from the reference EOS, the present molecular model and the molecular models from the literature. The number in parentheses indicates the statistical uncertainty<sup>a</sup> in the last digit.

	$T_c$ K	$\rho_c$ mol/l	$p_c$ MPa
EOS by Lemmon and Span <sup>10</sup>	508	4.7	4.7
Molecular model, this work	509 (3)	4.8 (1)	4.7 (2)
TraPPE model <sup>6</sup>	508	4.8	5.5
Modified TraPPE model <sup>7</sup>	508.2 (2)	4.74 (2)	4.85 (3)
AUA4 model <sup>8</sup>	512	4.8	
OPLS model <sup>9</sup>	526	4.7	5.6

<sup>a</sup> The statistical uncertainties were estimated by block averaging according to Flyvbjerg and Petersen<sup>41</sup> and the error propagation law. Note that the estimated uncertainties are very similar to the standard uncertainties.

Table 3: Pure substance parameters of the Peng-Robinson EOS.<sup>26</sup>  $T_c$  is the critical temperature,  $p_c$  the critical pressure and  $\omega$  the acentric factor.

Fluid	$T_c$	$p_c$	$\omega$
	K	MPa	-
Nitrogen	126.2	3.394	0.040
Acetone	508.1	4.701	0.309

Figure 1: Schematic of the experimental setup that was built for the present gas solubility measurements at high temperatures. VX indicates a valve, TX a thermometer and PX a pressure transducer. A: high pressure equilibrium cell, B: gauge-class, C: heating wire, D: copper cylinder, E: aluminum cylinder, F: vacuum chamber, G: gas bottle, H: high pressure spindle press, I: liquid reservoir, J: vacuum pump, K: endoscope.

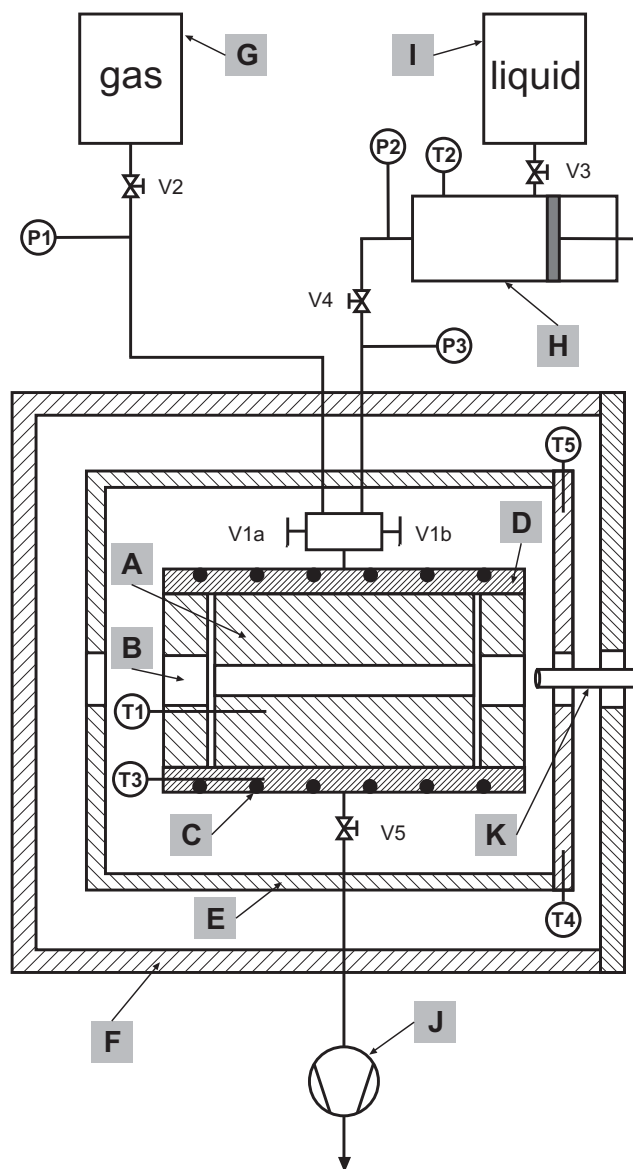


Figure 2: Saturated densities of acetone. Simulation data:  $\circ$  this work,  $\nabla$  TraPPE model,<sup>6</sup>  $\triangle$  modified TraPPE model,<sup>7</sup>  $\star$  AUA4 model,<sup>8</sup>  $\square$  OPLS model;<sup>9</sup>  $+$  experimental data;<sup>25,26</sup> — EOS by Lemmon and Span;<sup>10</sup>  $\blacktriangledown$  critical point of the EOS.<sup>10</sup>

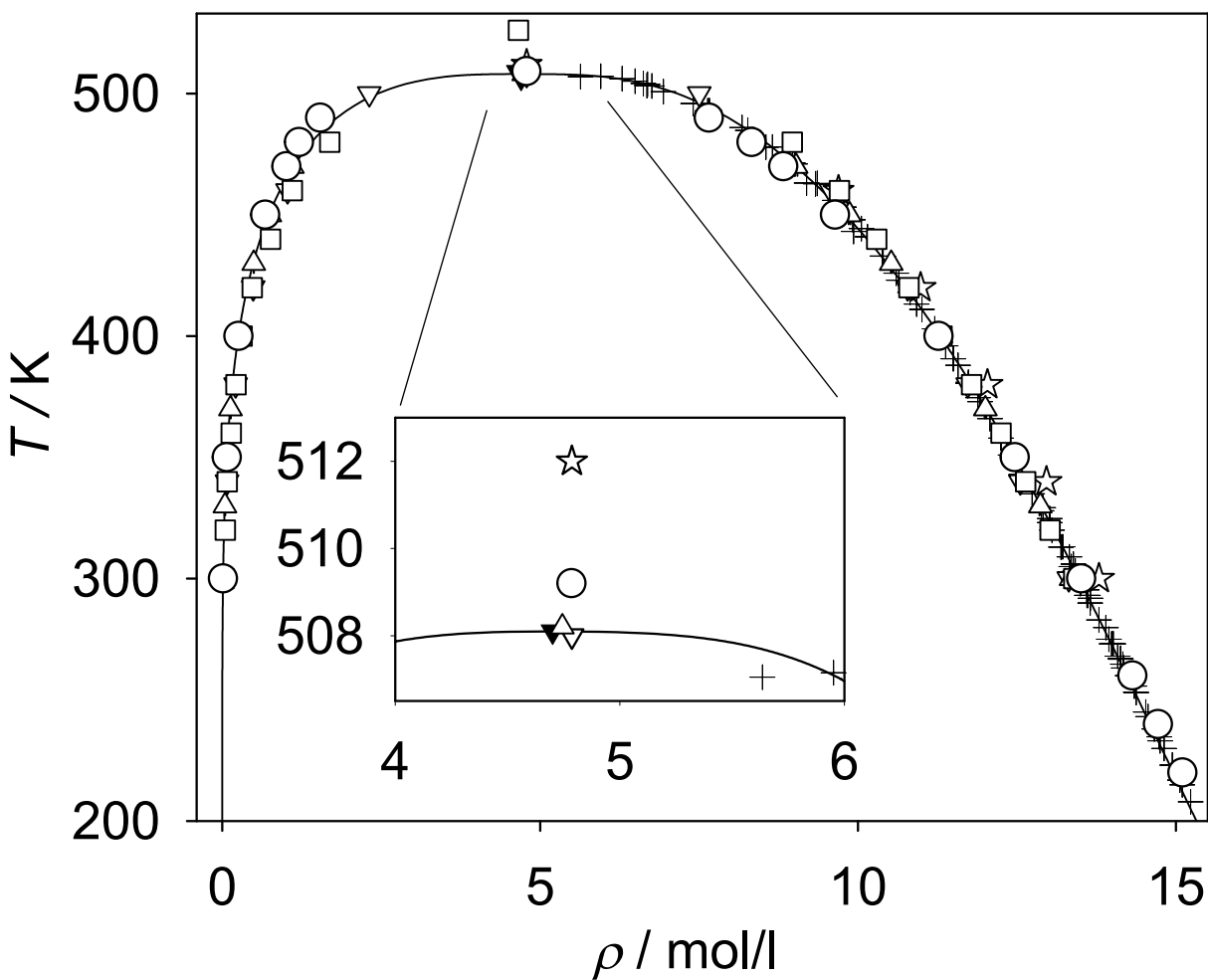


Figure 3: Vapor pressure of acetone. Simulation data:  $\circ$  this work,  $\nabla$  TraPPE model,<sup>6</sup>  $\triangle$  modified TraPPE model,<sup>7</sup>  $\star$  AUA4 model,<sup>8</sup>  $\square$  OPLS model;<sup>9</sup>  $+$  experimental data;<sup>25,26</sup> — EOS by Lemmon and Span;<sup>10</sup>  $\blacktriangledown$  critical point of the EOS.<sup>10</sup>

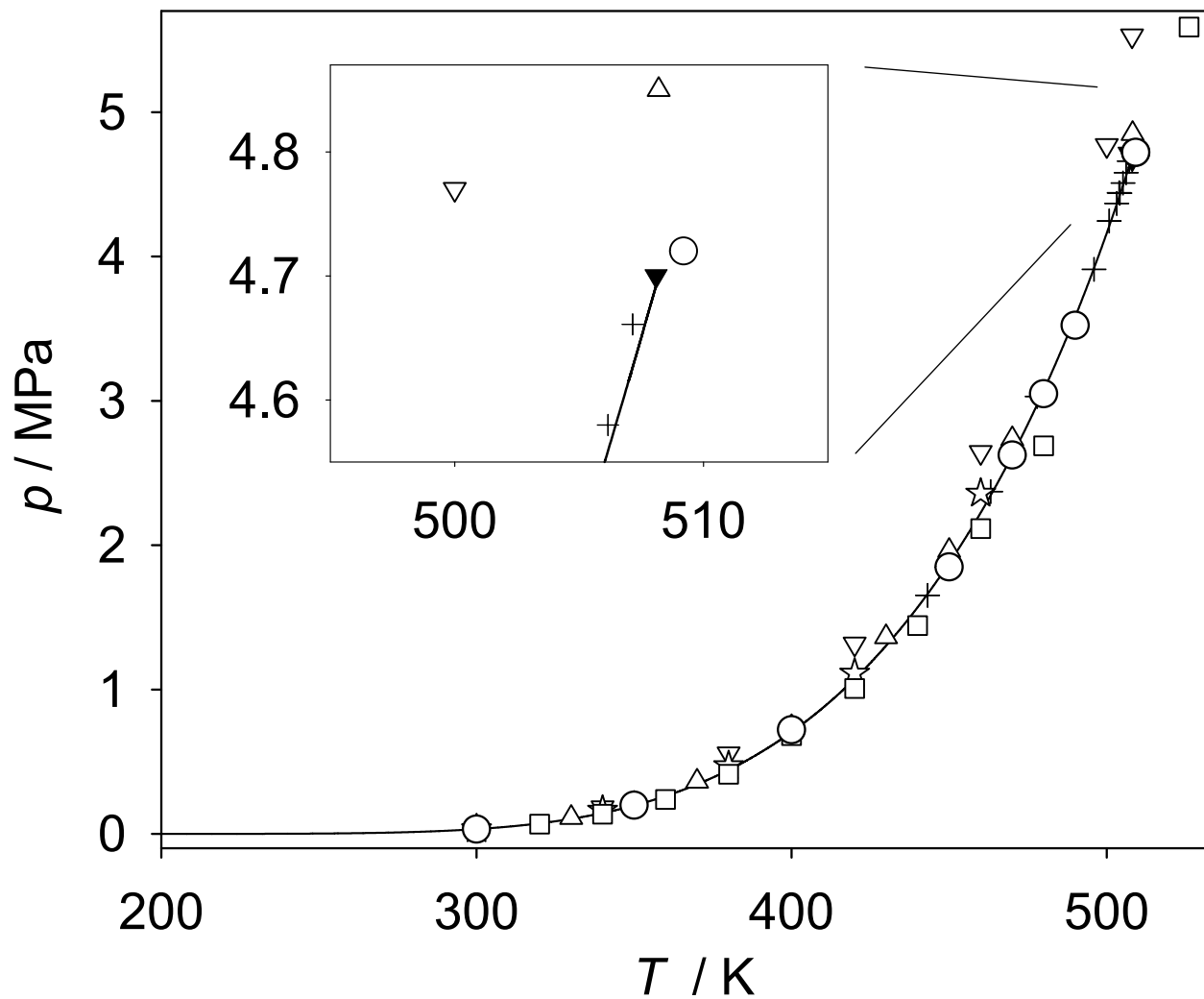


Figure 4: Heat of vaporization of acetone. Simulation data:  $\circ$  this work,  $\star$  AUA4 model;<sup>8</sup>  $+$  experimental data;<sup>25,26</sup> — EOS by Lemmon and Span.<sup>10</sup>

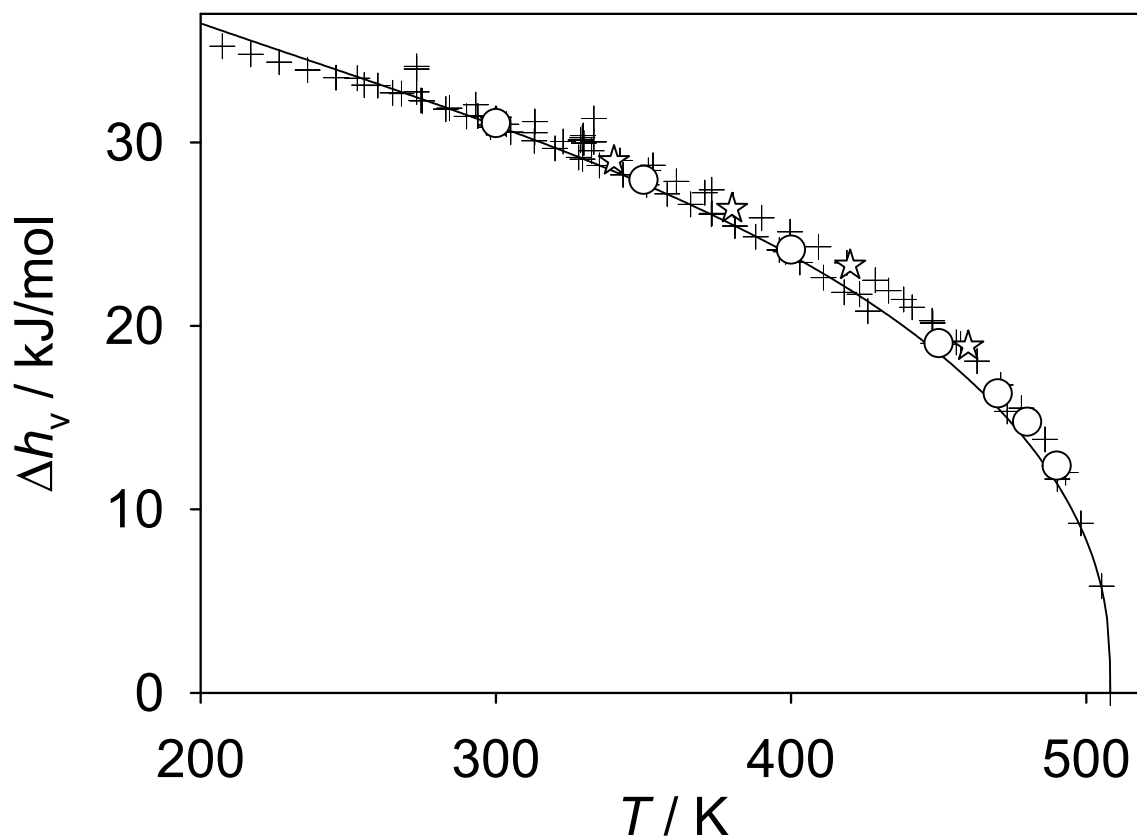


Figure 5: Relative deviations of vapor-liquid equilibrium properties of acetone from the EOS by Lemmon and Span<sup>10</sup> ( $\delta z = (z_{\text{sim}} - z_{\text{EOS}})/z_{\text{EOS}}$ ). Simulation data:  $\circ$  this work,  $\nabla$  TraPPE model,<sup>6</sup>  $\triangle$  modified TraPPE model,<sup>7</sup>  $\star$  AUA4 model,<sup>8</sup>  $\square$  OPLS model;<sup>9</sup>  $+$  experimental data.<sup>25,26</sup>

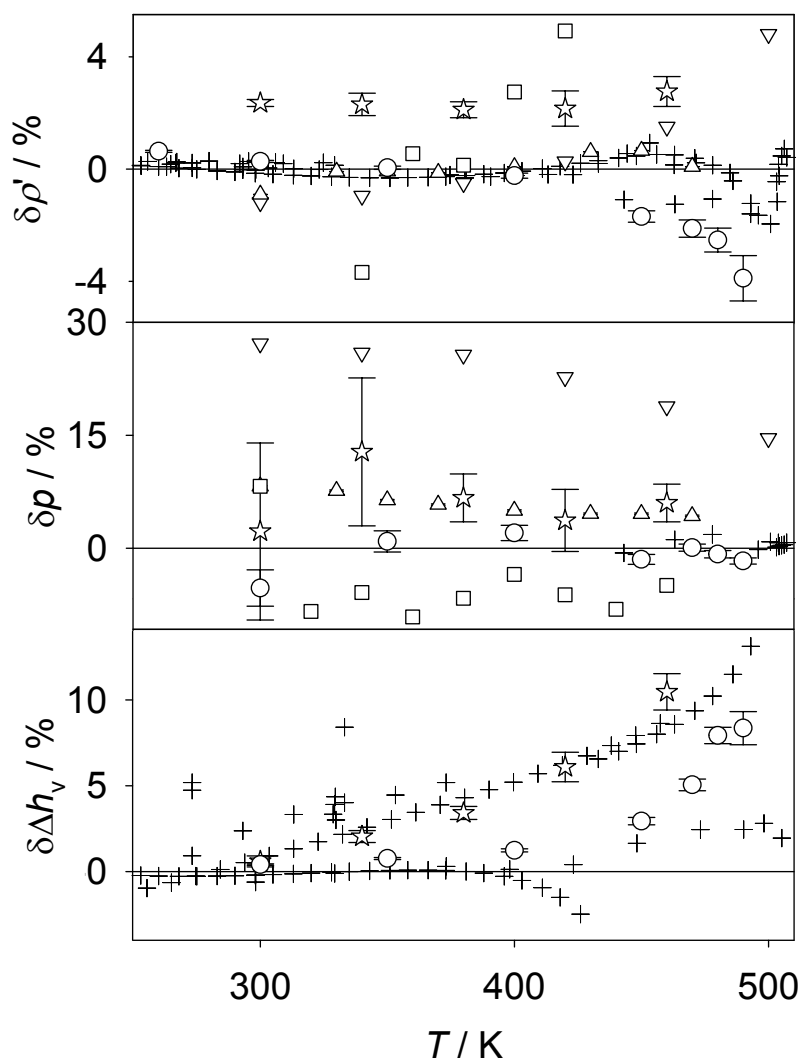


Figure 6: Density, speed of sound and residual enthalpy of acetone in the homogeneous region. Relative deviations between present simulation data and the EOS by Lemmon and Span<sup>10</sup> ( $\delta z = (z_{\text{sim}} - z_{\text{EOS}})/z_{\text{EOS}}$ ). The size of the bubbles indicates the magnitude of the relative deviation, the solid line is the vapor pressure curve.<sup>10</sup>

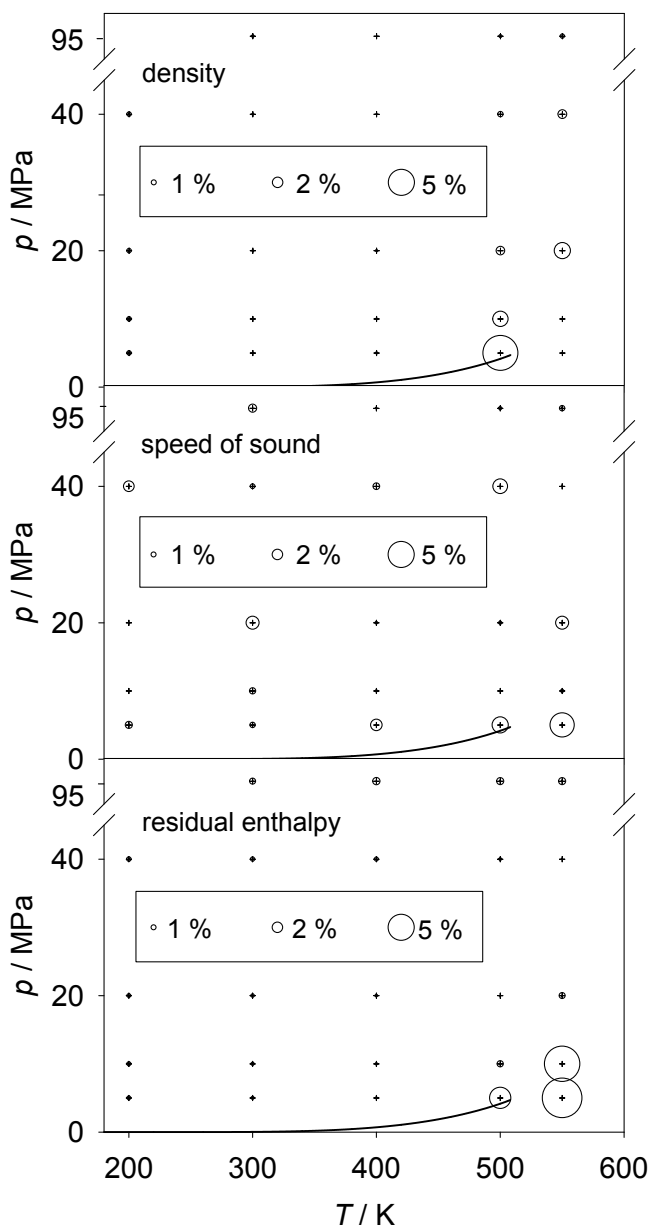


Figure 7: Second virial coefficient of acetone:  $\circ$  results from the present molecular model, this work;  $+$  experimental data;<sup>25,26</sup>  $\cdots$  correlation of experimental data from the DIPPR database;<sup>25</sup>  $—$  EOS by Lemmon and Span.<sup>10</sup>

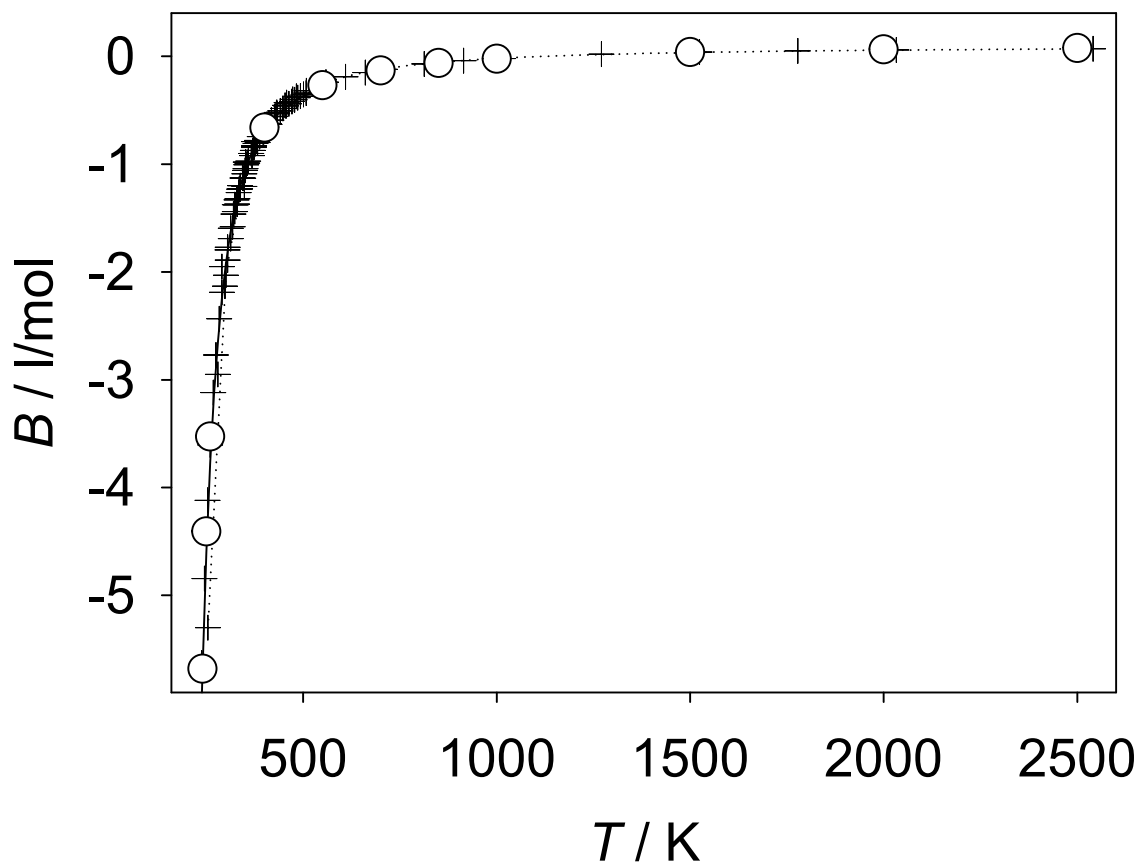


Figure 8: Self-diffusion coefficient of acetone along the saturated liquid line:  $\circ$  simulation data, this work; experimental data:  $\nabla$  McCall et al.,<sup>42</sup>  $\diamond$  Krüger and Weiss,<sup>43</sup>  $\star$  Holz et al.,<sup>44</sup>  $\triangle$  Wheeler and Rowley;<sup>45</sup> — correlation of experimental data by Ertl and Dullien.<sup>29</sup>

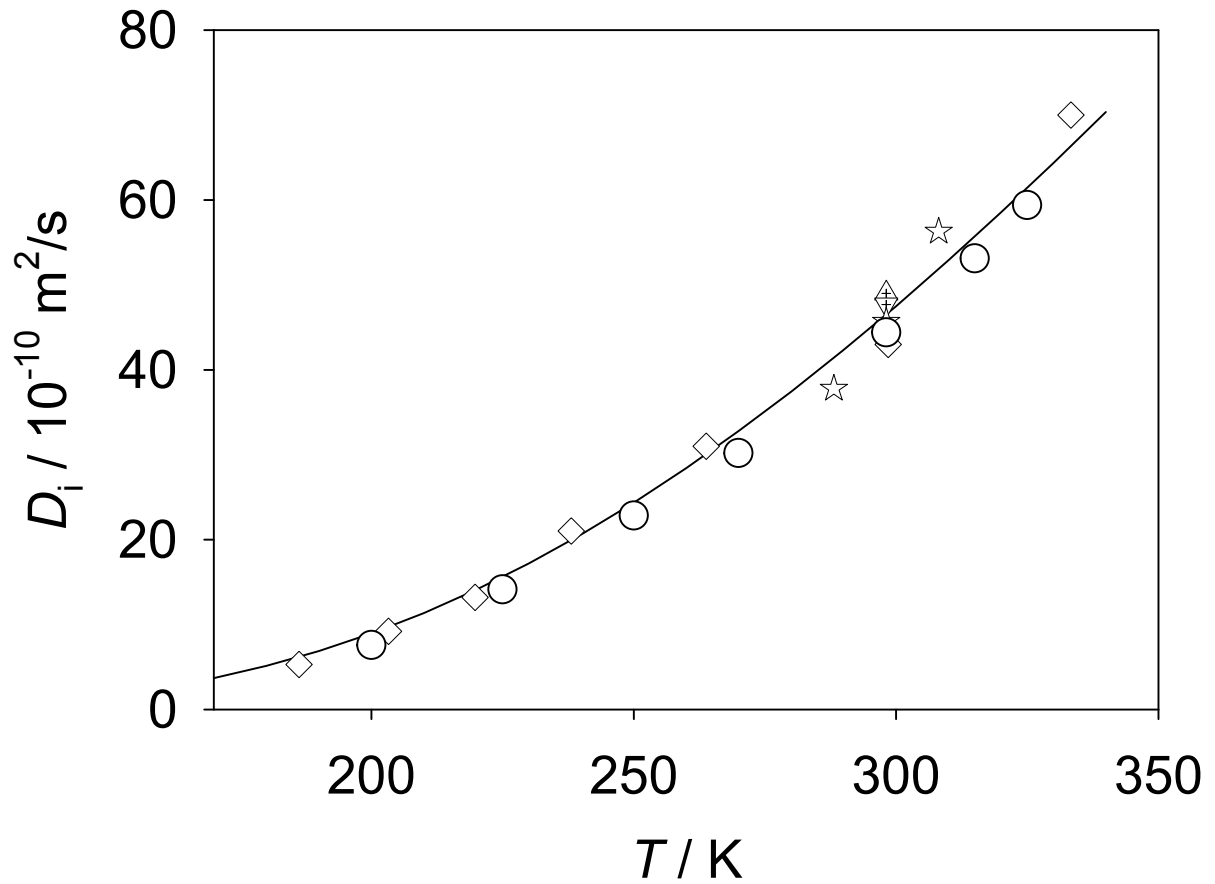


Figure 9: Shear viscosity of acetone along the saturated liquid line:  $\circ$  simulation data, this work;  $+$  experimental data;<sup>25,26,46</sup> — correlation of experimental data from the DIPPR database.<sup>25</sup>

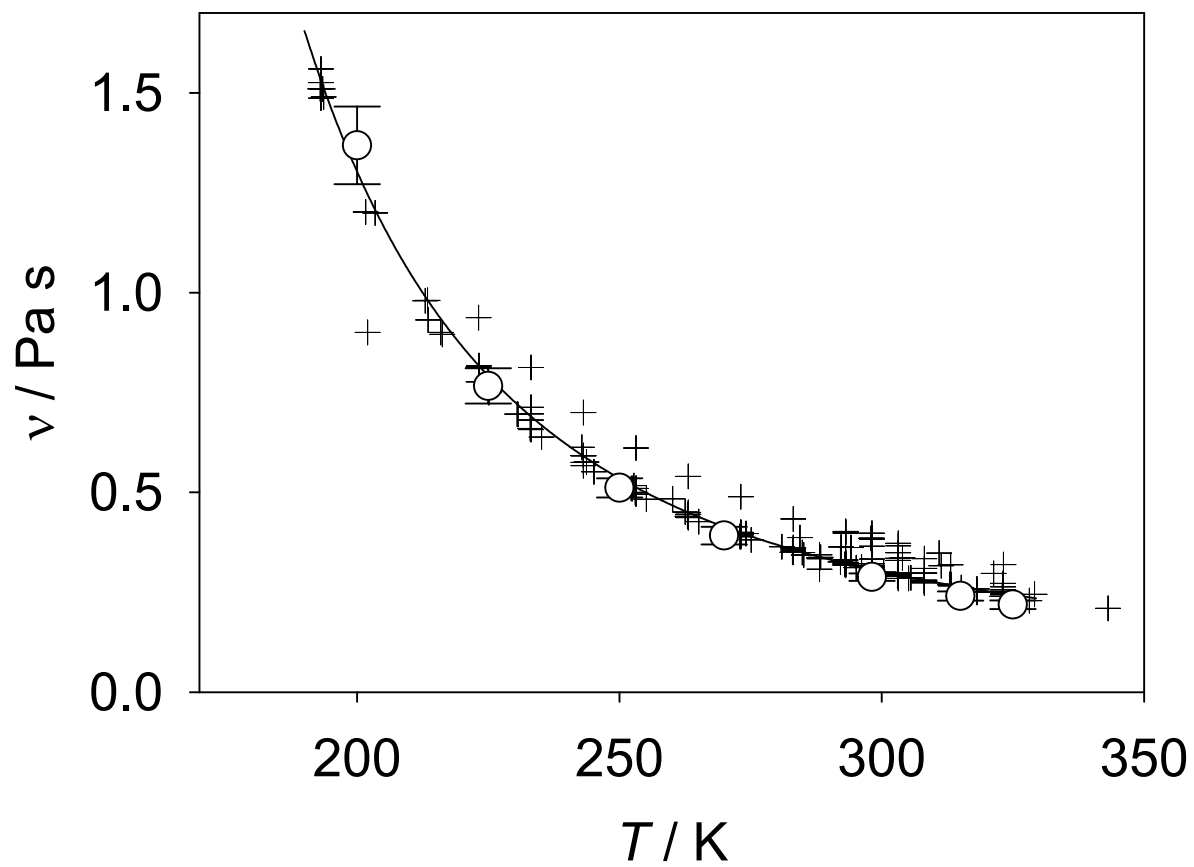


Figure 10: Thermal conductivity of acetone along the saturated liquid line:  $\circ$  simulation data, this work;  $+$  experimental data;<sup>25,26</sup> — correlation of experimental data from the DIPPR database.<sup>25</sup>

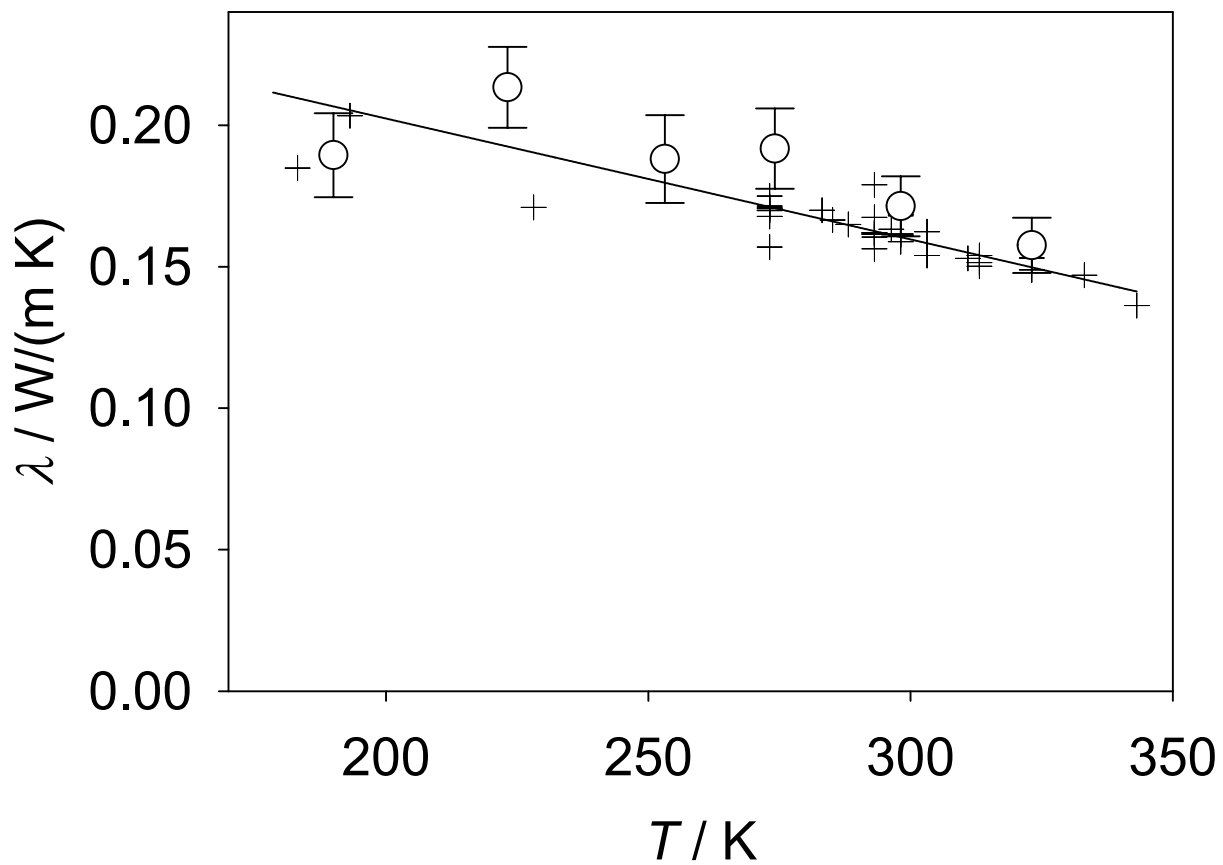


Figure 11: Saturated liquid line of nitrogen + acetone:  $\circ$ ,  $\bullet$  simulation data, this work;  $\diamond$ ,  $\blacklozenge$  experimental data by Windmann et al.;<sup>5</sup> —, - - - Peng-Robinson EOS (Huron-Vidal mixing rule). The dashed lines represent the same isotherms as the solid symbols.

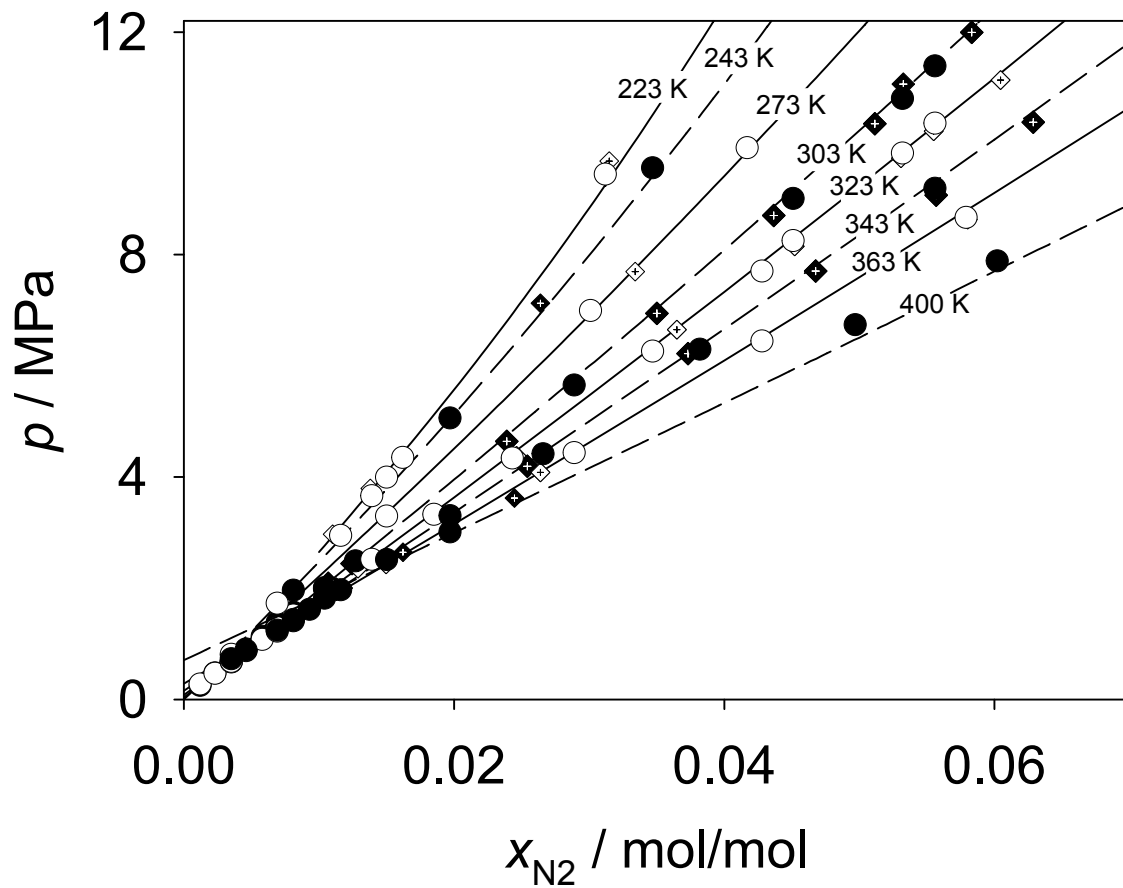


Figure 12: Saturated vapor line of nitrogen + acetone:  $\circ$ ,  $\bullet$  simulation data, this work;  $\diamond$ ,  $\blacklozenge$  experimental data by Windmann et al.;<sup>5</sup> —, - - - Peng-Robinson EOS (Huron-Vidal mixing rule). The dashed line represents the same isotherm as the solid symbols.

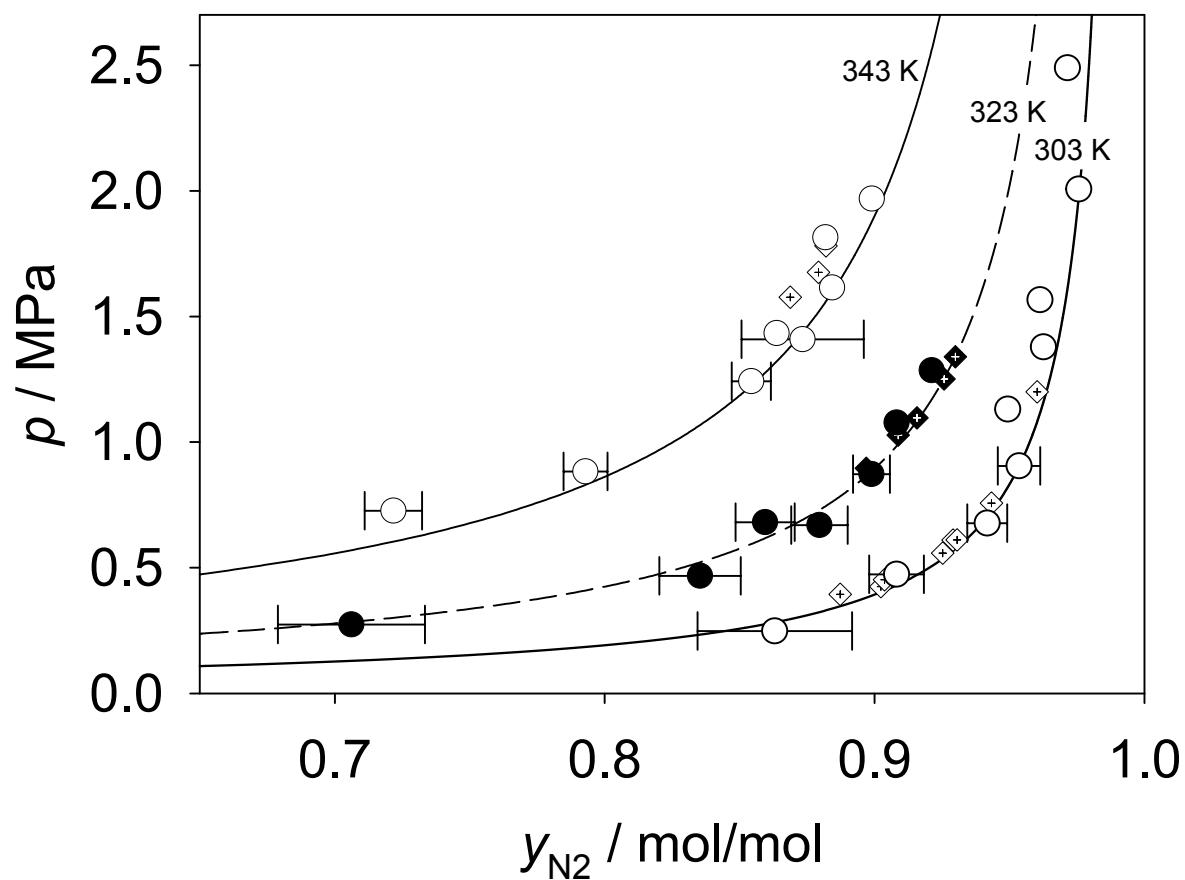


Figure 13: Henry's law constant. Nitrogen in acetone:  $\square$  Simulation data, this work; Experimental data:  $\boxplus$  Windmann et al.,<sup>5</sup>  $\blacktriangle$  Jabloniec et al.,<sup>47</sup>  $\bullet$  Just,<sup>48</sup>  $\star$  Horiuti,<sup>24</sup>  $\blacktriangledown$  Kretschmer et al.,<sup>30</sup>  $\blacksquare$  Nitta et al.,<sup>49</sup>  $+$  Vosmansky and Dohnal,<sup>50</sup>  $\times$  Tsuji et al.;<sup>51</sup> Oxygen in acetone:  $\circ$  Simulation data, this work; Experimental data:  $\oplus$  Windmann et al.,<sup>5</sup>  $+$  Levi,<sup>52</sup>  $*$  Fischer and Pfeleiderer,<sup>53</sup>  $\blacktriangledown$  Finlayson,<sup>54</sup>  $\star$  Horiuti,<sup>24</sup>  $\blacksquare$  Kretschmer et al.,<sup>30</sup>  $\bullet$  Schlaepfer et al.,<sup>55</sup>  $\blacklozenge$  Sinn et al.,<sup>56</sup>  $-$  Naumenko,<sup>57</sup>  $\blacktriangle$  Bub and Hillebrand,<sup>58</sup>  $|$  Tsuji et al.,<sup>51</sup>  $\times$  Luehring and Schumpe;<sup>59</sup> — straight line. All symbols above the dotted line represent nitrogen data, the others represent oxygen data.

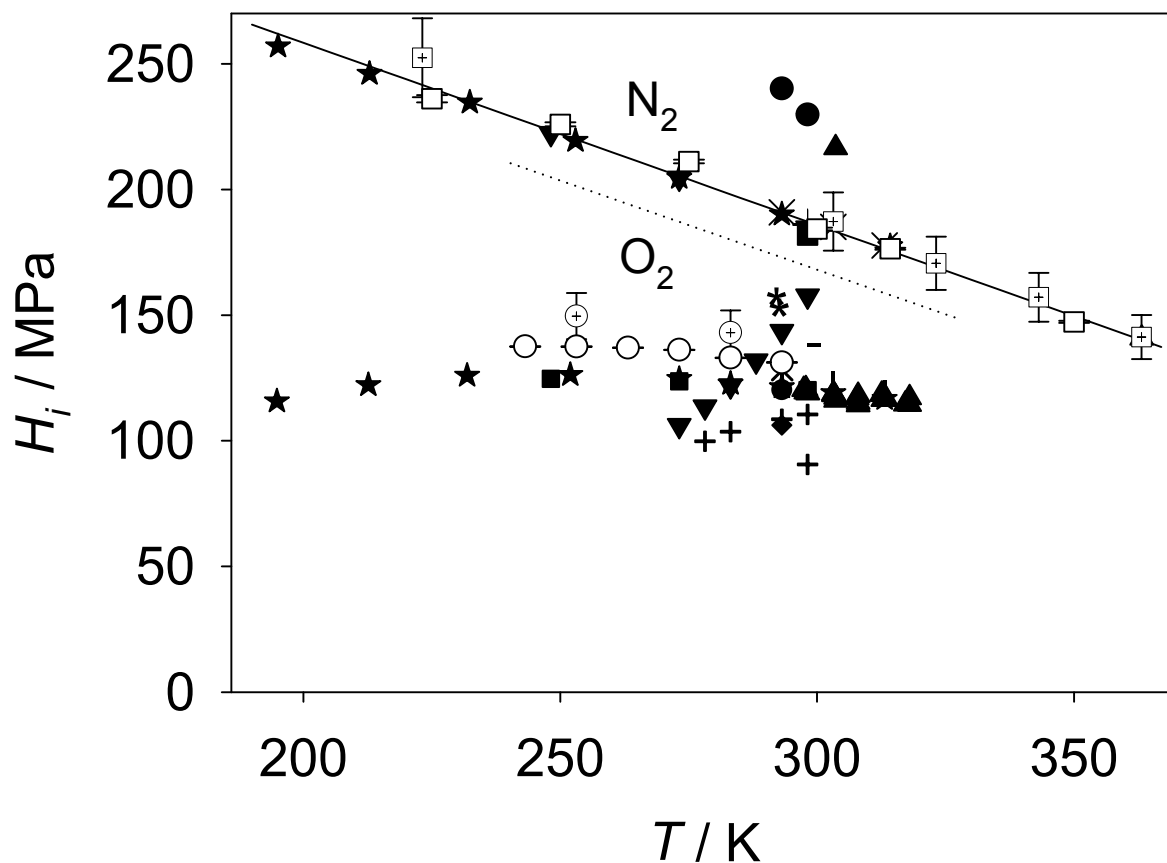


Figure 14: Saturated liquid line of oxygen + acetone: Simulation data, this work:  $\circ$  253.15 K,  $\bullet$  283.15 K; experimental data by Windmann et al.:<sup>5</sup>  $\diamond$  253.15 K,  $\blacklozenge$  283.15 K; —, - - - Peng-Robinson EOS with quadratic mixing rule.<sup>5</sup> The dashed line represents the same isotherm as the solid symbols.

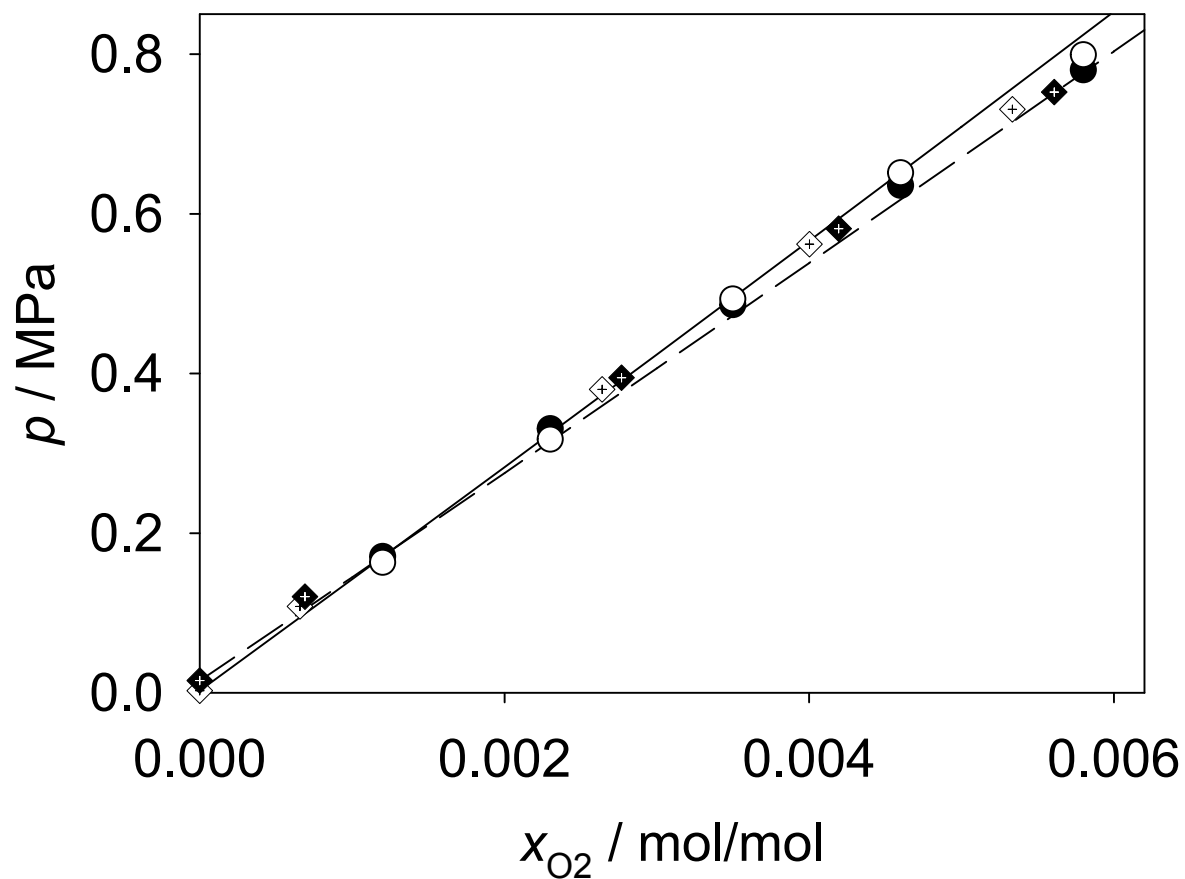


Figure 15: Vapor-liquid equilibrium of nitrogen + acetone around 400 K:  $\diamond$  experimental data, this work;  $\circ$  simulation data, this work; Peng-Robinson EOS: — Huron-Vidal ( $l_{ij}=241.9$ ,  $l_{ji}=926.5$ ), - · - quadratic ( $k_{ij}=0.1970$ ).

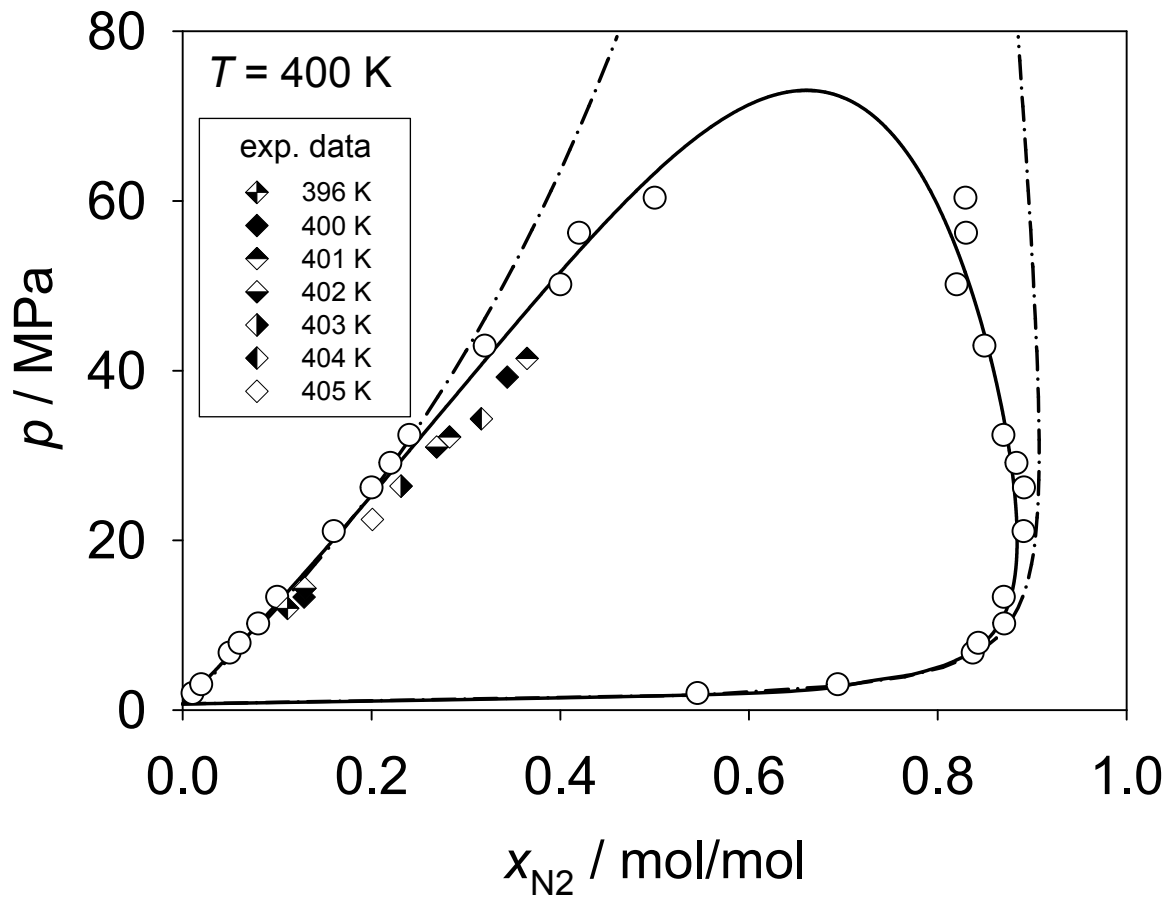


Figure 16: Vapor-liquid equilibrium of nitrogen + acetone around 450 K:  $\diamond$  experimental data, this work;  $\circ$  simulation data, this work; Peng-Robinson EOS: — Huron-Vidal ( $l_{ij}=-369.9$ ,  $l_{ji}=2200$ ), - · - quadratic ( $k_{ij}=0.0670$ ).

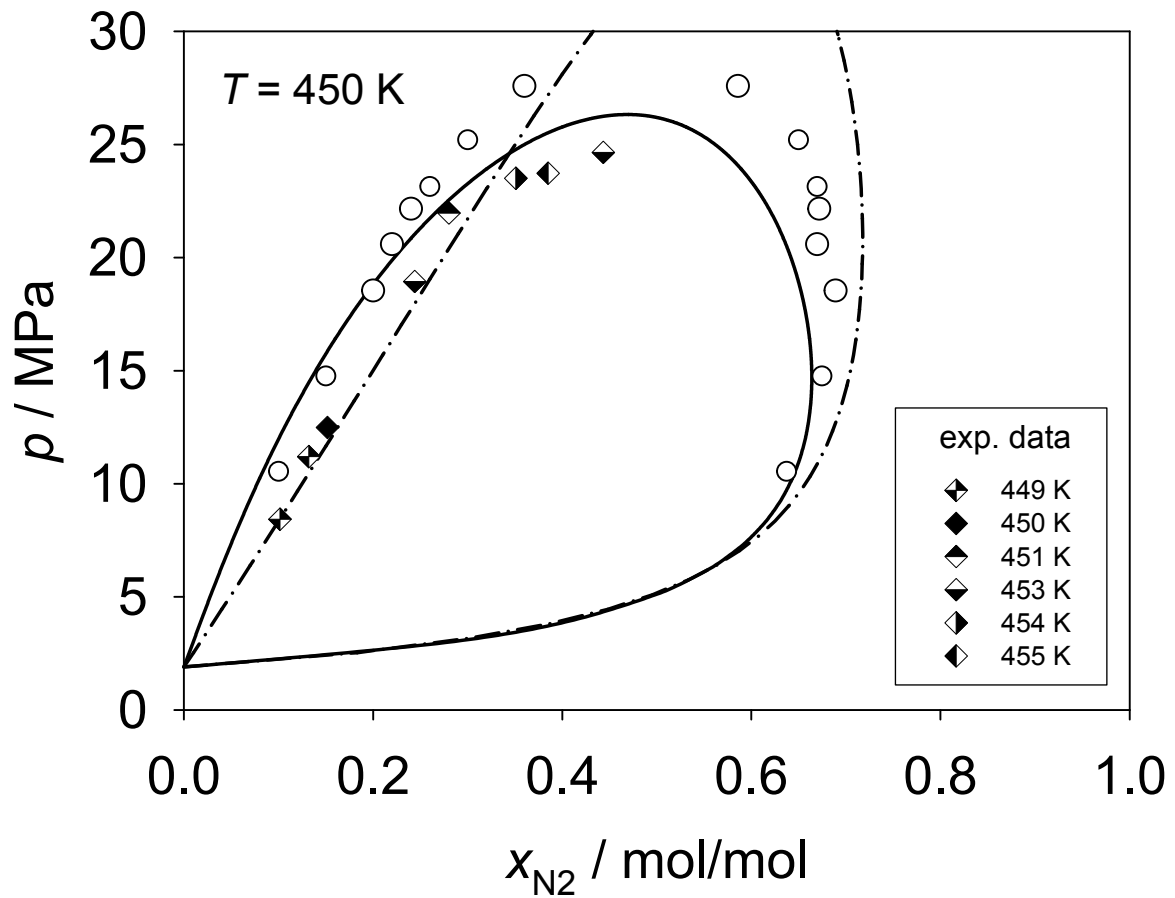
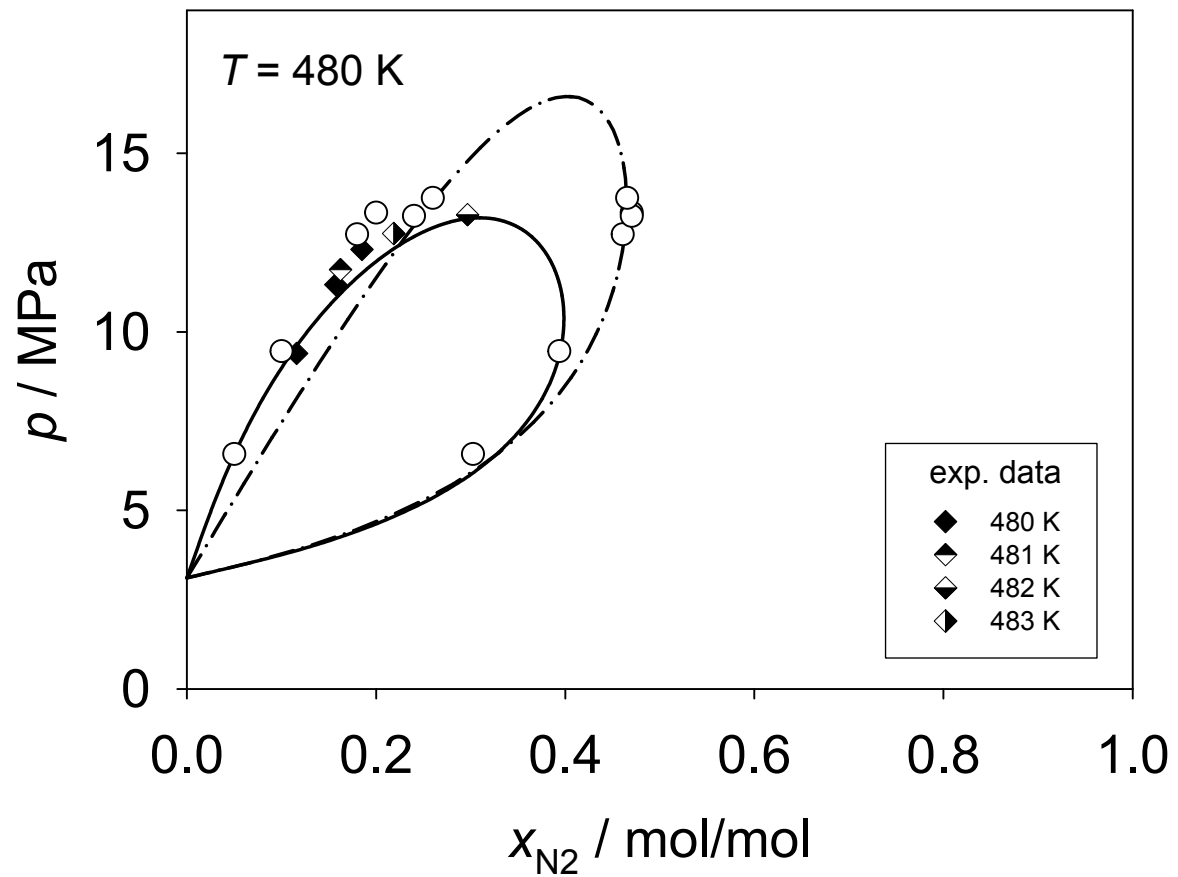


Figure 17: Vapor-liquid equilibrium of nitrogen + acetone around 480 K:  $\diamond$  experimental data, this work;  $\circ$  simulation data, this work; Peng-Robinson EOS: — Huron-Vidal ( $l_{ij}=-337.0$ ,  $l_{ji}=2964$ ), - · - quadratic ( $k_{ij}=0.0110$ ).



for Table of Contents use only. Title: Fluid phase behavior of nitrogen + acetone and oxygen + acetone by molecular simulation, experiment and the Peng-Robinson equation of state.

Authors: Windmann, Thorsten; Linnemann, Matthias; Vrabec, Jadran.

